Master Thesis

submitted within the UNIGIS MSc. programme
at the Department of Geoinformatics - Z_GIS
University of Salzburg, Austria
under the provisions of UNIGIS framework

Comparative evaluation of Microwave and Optical Images for Land Use and Land Cover Classification

by

Suman Baral
u105359

A thesis submitted in partial fulfilment of the requirements of
the degree of
Master of Science (Geographical Information Science & Systems) – MSc (GISc)

Advisor (s):

Him Lal Shrestha, PhD

Kathmandu, 2023

Science Pledge

By my signature below, I certify that my project report is entirely the result of my own work. I have cited all sources of information and data I have used in my project report and indicated their origin.

Nepal, 30 April 2023

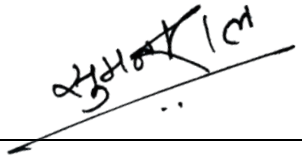

Place and Date	Signature

Acknowledgements

I am grateful to the University of Salzburg and my advisor, Dr. Him Lal Shrestha, for their encouragement and support throughout this project. Their timely encouragement and motivation were critical to completing my project within the time frame specified.

In this thesis, "Evaluation of S-1 and S-2 for LULC Classification," I had to overcome many difficulties in integrating two well-known remote sensing methods, optical and microwave, as well as the use of texture and dimension reduction. These difficulties included a lack of adequate resources online for the study, which occasionally made it difficult to advance with the thesis. Despite these difficulties, I was able to persist and gain important experience by finishing my thesis through constant support of my advisor.

Additionally, I would like to extend my sincere gratitude to my family (especially my wife Deepa), my tutor Mr. Prasidh Kandel, friends, and other close relatives for their unwavering moral support and encouragement throughout my academic career. Their support and confidence in my abilities served as a constant source of inspiration for me.

Abstract

The mapping of land use and land cover (LULC) is a significant and widely studied subject in academia. However, there hasn't been much research done on integrating optical and microwave data for LULC mapping, especially when combined with texture and dimension reduction methods. Additionally, little research has been done for LULC mapping in the Bhaktapur district. The study seeks to enhance knowledge by assessing the Sentinel-1 (S-1) as microwave data and Sentinel-2 (S-2) as optical data integration for high-accuracy LULC mapping in the Bhaktapur district. The study aims to evaluate the five LULC classes (agriculture, forest, fallow land, urban, and water) and the area covered by each. The results demonstrate that the integration of S-1 and S-2 data led to the allowable level of accuracy, with an overall accuracy (OA) of 91.06 percent and a Cohen's Kappa coefficient of 0.88. The S-1 data with principal component analysis (PCA) gave the least accurate results, with an OA of only 54.06 percent and a Cohen's Kappa coefficient of 0.36. Apart from S-1 and the integrated images classification, S-2 alone without the use of PCA and GLCM produced an OA of 83.07 percent and Cohen's Kappa coefficient of 0.77. The results show that using PCA and GLCM with S-1 improves accuracy, while using a similar approach with S-2 does not, demanding deeper investigation of the interactions between each principal component and texture measure. For both S-1 and S-2 image stacks, the RF Supervised Classification method was used, and the data was verified using a two-step hybrid approach. This involved validating any confusing cases in the field after first validating the results with high-resolution images of same date on the screen. The results of the study can be applied in numerous contexts. In terms of science, the findings back up advanced research on LULC mapping that uses PCA and GLCM on specific principal components or texture measurements to improve the classification accuracy of LULC. In terms of fundamental applicability, research fills in the gaps caused by a lack of accurate LULC data for decision-making by local level.

Keywords: LULC, microwave remote sensing, optical remote sensing, image integration

Table of Contents

List of Tables

List of Figures

List of Maps

List of Acronym and Abbreviations

DEM	Digital Elevation Model
ESA	European Space Agency
FC	False Color
GLCM	Grey Level Co-occurrence Matrix
GRD	Ground Range Detected
LC	Land Cover
LU	Land Use
LULC	Land use and Land Cover
OA	Overall Accuracy
PCA	Principal Component Analysis
RF	Random Forest
S-1	Sentinel-1
S-2	Sentinel-2
SAR	Synthetic Aperture Radar
SNAP	Sentinel Application Platform
SRTM	Shuttle Radar Topography Mission
VH	Vertical-Vertical
VV	Vertical-Horizontal

1. Chapter-1: Introduction

1.1. Background

Traditionally, LULC mapping were done manually using fieldwork or the interpretation of aerial photographs. However, due to their poor spatial and spectral resolution, these methods were time-consuming, labor-intensive, and frequently produced inaccurate results (Jensen, 2009). The efficiency, accuracy, and affordability of LULC mapping have all increased because of the development of remote sensing technologies (Jensen, 2009). For accurate mapping of LULC, remote sensing data like satellite images are crucial because they offer high-resolution spatial and spectral information.

Land use and land cover mapping has been utilizing optical and Synthetic Aperture Radar (SAR) as microwave remote sensing methods that offers more complete, accurate and reliable information on the many forms (Dong et al., 2009), but each data source has its own pros and cons. High spatial resolution information is provided by optical data, but cloud cover and other atmospheric factors can limit its usefulness (Aggarwal, 2004). On the other hand, SAR technique uses microwave radiation that can pass through clouds, making it an active imaging method that is unaffected by frequent cloud cover (Balzter et al., 2015). Additionally, SAR data is associated to the shape, texture, structure, and dielectric properties of the targets, and optical data is associated to the chemical, physical, and biological features of the targets, thus complementing each other in classification (Pereira et al., 2013).

There has been a significant amount of research on LULC studies and applications to cope with climate change and sustainable development (Chang et al., 2018) in the domain of monitoring climate change, environment management, urban planning etc. Currently, LULC research in the field of remote sensing is focused on using optical or SAR imagery but in recent years the integration of these two data sources has drawn more attention as a way to combine data from various images to produce more accurate results (Dong et al., 2009).

The study is intended to use optical and microwave SAR data from S-1 and S-2 respectively in order to respond research questions. To categorize the LULC classes, the study employs a random forest (RF) classification which is a machine learning-based classification approach. The study's findings will aid in the creation of LULC mapping techniques that integrate data from different sensors in order to be more accurate and reliable. Additionally, the research will cover the advantages and disadvantages of combining multi-sensor data for LULC mapping. The dimension reduction and texture measure will support the integration for LULC classification in an effort to test whether they can improve LULC's accuracy. Combinations of Sentinel-1 (S-1), Sentinel-2 (S-2), integrated images, and their principal component analysis (PCA) and grey level cooccurrence matrix (GLCM) will be used in the methodology.

Bhaktapur district is recognized for its rich cultural heritage, which includes ancient temples, palaces, and homes built in the Newari architectural style (Silva, 2015). However, the region also has to deal with a number of environmental problems, including as increasing urbanization, degraded soil, contaminated water, and natural disasters (Welton-Mitchell et al., 2017; Thapa Chhetri & Moriwaki, 2017). Therefore, the significance of the study area as Bhaktapur lies in the complex and difficult background it offers to LULC mapping. There are urban areas, farms, and hills covered in forest in the district, which has a very diverse geology, climate, and land use patterns. In order to manage those land sustainably and counteract the effects of climate change, it is essential to map LULC accurately and completely.

The study is notable for various reasons. The first benefit is that it advances the multi-sensor data integration of LULC mapping techniques, which can improve understanding of the extent and distribution of different LULC classes. The project will also shed light on the advantages and disadvantages of combining data from multiple sensors for LULC mapping. It informs the scientific communities, policy makers and practitioners about the potential benefits of using multi-sensor and SAR data integration for sustainable development and climate change especially in context of Bhaktapur district.

1.2. Objectives

1.2.1. Main Objective

The main objective of this study is to explore the potentiality of combining multi-sensor optical and microwave SAR data for comprehensive LULC classification.

1.2.2. Specific Objectives

The study's specific objectives are;

- To explore the use of texture and dimension reduction for LULC mapping.
- To evaluate and compare the LULC classification accuracy using multi-sensor optical and microwave SAR images.
- To identify the benefits and constraints of integrating multi-sensor optical and microwave SAR images for LULC mapping.

1.2.3. Research Questions

The research aims to answer the following questions:

- How much can the accuracy of LULC classification be increased by integrating multi-sensor optical and microwave SAR images?
- What are the benefits and drawbacks of integrating multi-sensor optical and microwave SAR images for LULC mapping?
- What will be the effect on classification accuracy using texture and dimension reduction methods?

1.3. Area of Focus

The study focuses on contrasting the land use and land cover (LULC) random forest (RF) classification method utilizing optical, SAR, and their integration hoping to fulfill the several research gaps scientifically and geographically. Geographically to provide the LULC results that support the district's use of evidence-based decision-making, scientifically by using

dimension reduction techniques like principal component analysis (PCA) and textural measures like the grey level cooccurrence matrix (GLCM). It initially assesses the reliability, accuracy, and effectiveness of various methods and data sources. It then looks at the role that visual element like texture, shape, and spectral data have in LULC mapping. Thirdly, it combines several data sets to analyze the best LULC mapping methods and parameters.

1.4. Literature Review

1.4.1. Land Use and Land Cover and its Applications

Cihlar et al. (2001) describes, the terms land cover (LC) and land use (LU) refer to the basic elements that represent natural and anthropogenic activities on the Earth's surface, respectively. Forests, glaciers, rivers, open water, bare soil, and rock are examples of natural LC features. In contrast, human endeavors like building roads, buildings, and water storage facilities result in LC. In order to serve a specific purpose, LC is typically divided into discrete categories based on the physical characteristics of the Earth's surface. Contrarily, LU describes how people use these material possessions.

Kumar & Singh (2021) describes, timely and precise LULC change detection is essential for the macro and micro level sustainable development of any location. Within the domain other several applications have been explored using these techniques, including forestry and agriculture (Gilmour & Nurse, 1991; Virgo & Subba, 1994), ecosystem services (food production, carbon storage, and habitat quality) (Rimal et al., 2019), on soil organic carbon stocks (Bae & Ryu, 2015), urban sprawl (Salem et al., 2020), climate change impacts (Chen et al., 2020) etc.

1.4.2. Land Use and Land Cover Classification System

Establishing a classification strategy is the initial stage in any study involving classification. Whatever the selected system of classification, each class needs to have a precise and well-supported definition. Using a pre-existing classification system has the benefit, making comparisons to other maps that employ the same system simpler.

Anderson (1971) has defined the standards and need of LULC classification schemes. FAO (2023) has defined the LC classification system design criteria. *Corine Land Cover Classes* (2023) has defined the hierarchy of LC classes along with its definition.

The following requirements should be met by a LULC classification system in order to successfully use satellite remote sensing data prescribed by Anderson (1971):

i. Using data from distant sensors, LULC categories should be identified with an accuracy of at least 85 percent.
ii. The accuracy of interpretation for the different categories should be generally equivalent.
iii. Repeatable or recurrent results ought to be possible from one interpreter to another and from one sensing time to another.
iv. The classification system must be applicable in a variety of circumstances.
v. The classification should permit the substitution of vegetation and other forms of LC for activities.
vi. Utilizing information gathered all year round from remote sensors, the classification algorithm must function.
vii. It must be possible to aggregate categories.
viii. Comparisons of land use data from the future should be possible.
ix. Wherever possible, classification should be utilized for a range of purposes.

1.4.3. History of Land Use and Land Cover in Nepal

Land use and land cover classification and change detection have a long history in Nepal. The first attempt at LULC mapping was conducted by Nepal's Forest Resource Survey Office (FRSO) in 1964, which produced a countrywide map of the forest cover based on aerial images taken in 1953–1958 and 1963–1964 periods. For the purpose of classifying forest land as either commercial or noncommercial, the FRSO used visual interpretation of these images together with field verification (Acharya et al., 2010). The first thorough LULC mapping was carried out in 1986 by the Land Resource Mapping Project, LRMP (1986)

using aerial images taken in 1978–1979 at a scale of 1:50,000. Numerous datasets related to geology, the land system, land use, and land capability are produced by this research. Gilmour et al. (1991) conducted an analysis of changes in tree cover that are occurring on the different land classes in a 14,000 ha catchment region near Kathmandu discovered there are strong indicators that the entire landscape is experiencing a sustained afforestation process at the hands of the farmers. Virgo et al. (1994) examined the shift in land use in eastern Nepal's Koshi hills between 1978 and 1990. The method proved to be quick and accurate enough to identify changes in farm-level land usage in sharply dissected mountain terrain. Uddin et al. (2015) produced first and most complete national land cover database of Nepal using 2010 Landsat TM data.

Over the past few decades, LULC in Nepal has undergone constant change as a result of substantial changes caused by anthropogenic and natural causes and their influence on the local, national, and regional environment and climate (Paudel et al., 2016). Haack & Rafter (2006) conducted an analysis of the urban changes in the Kathmandu Valley as well as a look at how the maps were made and what was on them. Bhaktapur is also no exception to this case, there has been much LULC changes (Thapa Chhetri & Moriwaki, 2017), further researches include - in 1988, the Bhaktapur district had a forest cover of around 42.5 percent, 53.3 percent agricultural or shrubland, 1.8 percent built up, and 2.2 percent bare soil. In 2001, 33.8 percent of the area was forest, 53.7 percent used for agriculture or shrubs, 7.7 percent occupied by buildings, and 4.6 percent left with bare soil. Forest coverage was estimated to be around 37 percent in 2010, followed by agricultural and shrub land at 29.4 percent, built-up areas at 11.12 percent, and bare soil at 22.40 percent. The land categories in 2015 included roughly 30.1 percent as forest cover, 36.7 percent as agriculture or shrubs land, 24.0 percent as built-up areas, and 9.0 percent as bare soil.

1.4.4. Microwave and Optical Remote Sensing and it’s Integration

Alfrey (1981) describes remote sensing as the process of viewing the surface of the Earth from a plane or satellite while analyzing changes in Earth's Reflectance as a function of wavelength in the optical and adjoining spectral ranges. Wong et al. (2021) explains how the field of remote sensing has swiftly developed since the launch of the first Earth Observation Satellite, Landsat, in 1972, with improvements in the methods and techniques for information extraction and ground resolution of satellite images.

Swift et al. (1980) defines, microwave remote sensing is the process of examining the data gathered by sensors that operate in the microwave region of the electromagnetic spectrum. Wavelengths in the vicinity of 1 mm to 1 m are included in the microwave section of the spectrum. While visual, near-infrared, and short-wave infrared sensors are used in optical remote sensing to create images of the Earth's Surface by observing the Sun Radiation reflected from objects on the ground.

The microwave and optical remote sensing have different strengths and weaknesses. Microwave remote sensing is advantageous because microwaves can penetrate clouds and provide an unobstructed view of the Earth's Surface, while optical remote sensing is advantageous because it has high spatial resolution and sensitivity (Balzter et al., 2015) Swift et al. (1980) discussed the various uses for microwave remote sensing, such as determining the age of polar ice, ocean temperature and salinity, winds over the ocean, and soil moisture through vegetation. Staelin & Kerekes (1995) evaluated the microwave and optical remote sensing methods used in conjunction, which can offer higher retrievals of atmospheric parameters.

Optical and microwave remote sensing can be used together to improve LULC classification. Zhang et al. (2020) proposed a feature-level fusion framework for LULC classification in overcast mountainous regions using a combination of Landsat Operational Land Imager (OLI) and Advanced Land Observing Satellite-2 (ALOS-2) images and obtained an accuracy of over 85 percent. Chachondhia et al. (2021) used optical and

microwave data to evaluate the effectiveness of machine learning algorithms, it was discovered that the combination of microwave and optical led to more accurate LULC classification findings. Khan et al. (2020) evaluated the fusion technique for Sentinel-1 (S-1) and Sentinel-2 (S-2) to achieve high LULC mapping accuracy in order to assess the area occupied by the negative landforms and found the result to achieve 84 percent overall accuracy (OA).

Several studies have compared the accuracy of LULC classification using multi-sensor data to using individual optical or SAR data. For example, in a study by Tavares et al. (2019), the change in LC was compared by the authors using optical, SAR, and their fusion. According to the results, the integration of S-1 and S-2 data had the highest OA, which was 91.07 percent. S-2 data alone produced an OA of 89.53 percent, followed by S-2 data combined with radiometric indexes, which produced an OA of 89.45 percent. Using only S-1 data, however, yielded the lowest accuracy, with an OA of 56.01 percent. Similar studies by Khan et al. (2020) and Clerici et al. (2017) etc. have shown the similar results.

A study by Chatziantoniou et al. (2017) concludes, the most accurate findings were obtained by integrating different spectrum information to help with classification implementation, increasing Cohen's Kappa from 0.894 to 0.928 and total accuracy from 90.83 to 93.85 percent. Valdivieso-Ros et al. (2023) likewise, came to the conclusion that the integration does not significantly improve class accuracy. There may be a number of factors to consider while choosing the classification algorithms, training samples, etc. e.g. Chatziantoniou et al. (2017) used Support Vector Machine.

1.4.5. Random Forest as Machine Learning Classifier

Gislason et al. (2004) describes random forest (RF) as a classifier that produces a large number of classification trees. The approach basically looks across a random fraction of the variables at each node to find a split for each tree, which is trained using a bootstrapped sample of the training data. In a RF, the input vector is fed into each tree in the forest as an input, and the supervised classification is then decided by a majority vote.

The studies suggest that RF is an accurate method for predicting LULC using S-2 data. Tavares et al. (2019) found that while integrating S-1 and S-2 data for LULC classification in Belém, Brazil, a RF classifier attained an OA of 91.07 percent. Svoboda et al. (2022) achieved a Cohen's Kappa of 0.84 and an OA of 89.1 percent for the Czech Republic's LULC classification using S-2 data. Srivastava et al. (2022) studied the performance of four supervised machine learning algorithms and discovered that RF had the highest accuracy, with S-2 data sets having an accuracy of 91.45 percent and Landsat 8 data sets having an accuracy of 95.86 percent. Nurfadila et al. (2019) found that the LULC extraction over the Enrekang Region had a 95 percent OA using the RF algorithm on multitemporal S-2 data.

1.4.6. Use of Textures and Dimension Reduction for Classification

Using principal component analysis (PCA) can improve the accuracy of LULC classification. Comber et al. (2016) discovered that classification accuracy was enhanced by using ranked scores and spatially weighted PCA loadings as textural inputs. Makar & Shahin (2022) used PCA to create a SC strategy for S-2 images, with an OA of 86.8 percent. Choi et al. (2014) used Aerial hyperspectral sensors to apply PCA, and it was discovered that the first and second bands of the PCA-transformed image had the highest accuracy for classifying LC. Deng et al. (2008) obtained an OA of 89.54 percent when using PCA to detect land-use changes in an urban context. These results imply that PCA can be a useful technique for increasing LULC classification accuracy.

It is suggested in literature, the GLCM plays a role in LULC classification. Tassi & Vizzari (2020) performed object-oriented classification of LULC using the GLCM and machine learning techniques, achieving high accuracy. Kumar et al. (2013) used artificial neural networks (ANN) to identify Landsat ETM+ data using the GLCM, spectral data, and topographic data. While Vivekananda et al. (2021) used multi-temporal image analysis to find variations in LULC across time, which might be supported by GLCM analysis, but does not directly address the role of the GLCM. The attempts are made employing either ANN,

Convolution Neural Networks or OOC, the use of GLCM in pixel-based machine learning algorithm like RF needs to be evaluated.

1.4.7. Accuracy Assessment

Without an accuracy evaluation, no LULC classification effort would be complete (Cihlar, 2000). Further (Cihlar, 2000) explains, the degree to which the map agrees with the reference LULC classification indicates how accurate the classification is (i.e., ground condition). The error matrix and Cohen's Kappa are widely used standard means of classification accuracy assessment since it has many attractive features as an index of classification accuracy (Foody, 2002). Apart from the OA, the individual class accuracies are measured by user and producer accuracy. The ability to classify the various real-world LULC categories is measured by the producer's accuracy, which counts errors of omission while a classified pixel's likelihood of matching the type of LULC at its associated real-world location is represented by the user's accuracy, which quantifies errors of commission (Campbell & Wynne, 2011; Jensen, 1996 ; Congalton, 1991).

There are several factors that affect the accuracy of LULC classification. Markham & Townshend (1981) described a relationship between classification accuracy and spatial resolution, with coarser resolutions resulting in lower accuracy. Smith et al. (2003) discovered that LULC heterogeneity and patch size both influence classification accuracy, with larger patches and less heterogeneity resulting in higher accuracy. Khatami et al. (2016) did a meta-analysis and discovered that adding texture information, auxiliary data, multi-angle, and time images enhanced classification accuracy, whereas spectral information manipulation techniques including feature extraction and index construction showed less significant gains.

The standard error matrix-based studies, which have been used to assess map accuracy, have worked well with the basic sample designs that have been used (Stehman, 2009). A probability sampling technique used in sample surveys is stratified sampling. The components of the target population are separated into distinct groups or strata, and within

each stratum, they are similar to one another in terms of a few key survey-relevant criteria. Additionally, stratification is utilized to improve the effectiveness of a sample design in terms of survey costs and estimator accuracy (Parsons, 2017). The usual justification for stratifying by map class is to give rare classes a disproportionate sample size with the aim of precisely estimating the class specific user accuracy (Stehman, 2009).

1.5. Study area

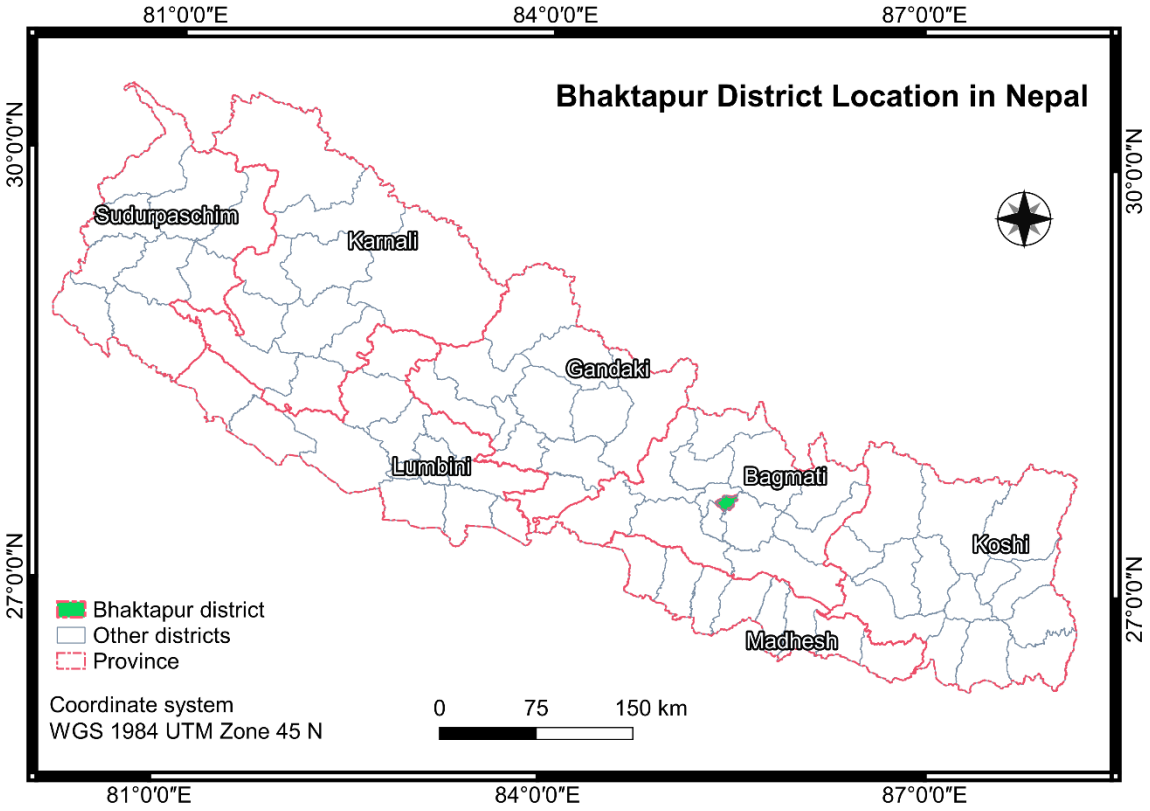

Map 1.1: Bhaktapur district location in Nepal

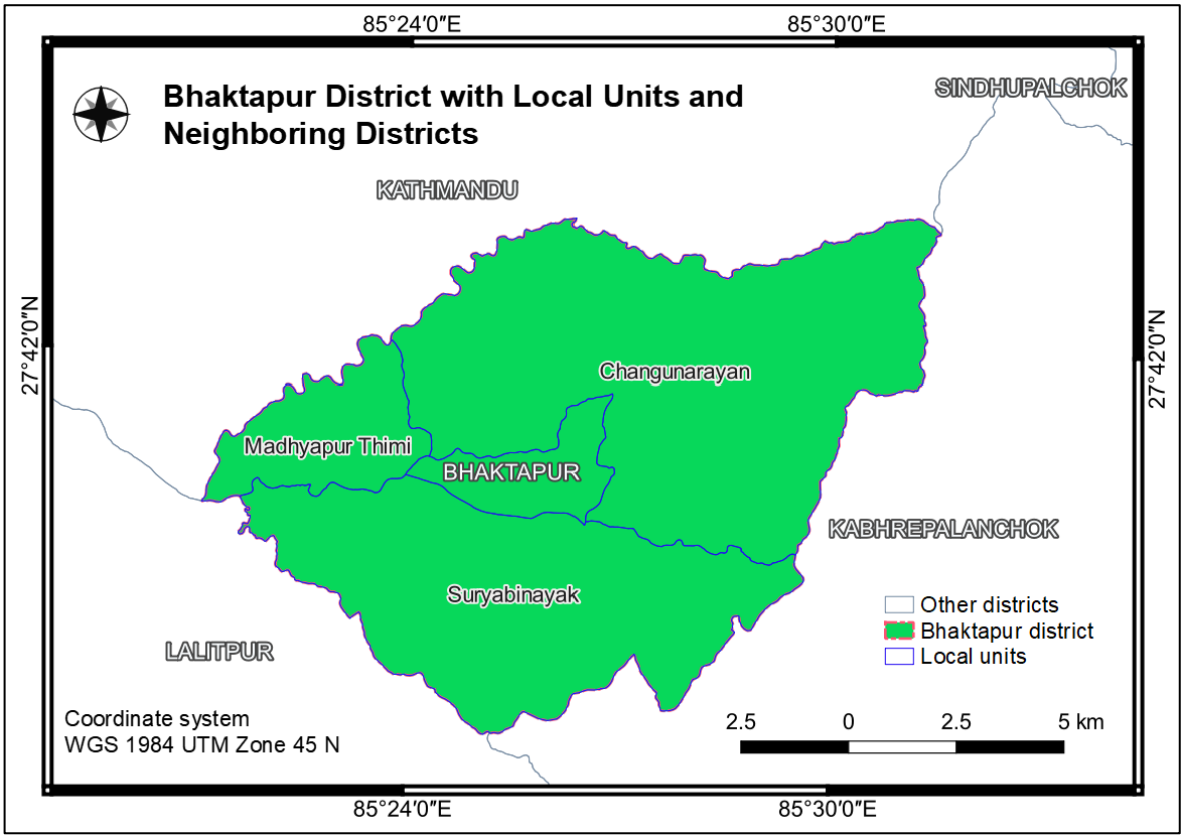

Map 1.2: Bhaktapur district with local units and neighboring districts

1.5.1. Geographic Description

Bhaktapur District is located in the Bagmati Province of Nepal. It is situated in the eastern part of the Kathmandu Valley and is surrounded by the districts of Kavrepalanchowk to the east, Sindhupalchowk to the north, Lalitpur to the south, and Kathmandu to the west. The district's 119 square kilometer population is 4,32,132 (NSO, 2023).

The altitude of Bhaktapur is between 1,331 meters and 2,191 meters above the sea level. The district is bounded by the latitudes 27.624 N and 27.764 N (Eastern) and longitudes 85.399 E and Longitude 85.539 E. A few of the rivers and streams that traverse the district's varied landscape of hills and valleys include the Hanumante River and Manohara River.

Bhaktapur district is distinguished geographically by a variety of LULC patterns, ranging from newly and historical urban areas to diverse agricultural fields and forested hills (DDC Bhaktapur, 2023). The district's geographic characteristics are largely similar to those of Lalitpur District and Kathmandu District, the other two districts in the Kathmandu valley. Hills

from the Mahabharata series cover the whole eastern section of the district as well as roughly half of the northern and southern regions. Nepali is the official language of the Bhaktapur district. However, there is a significant Newari community in the district, and they have their own language, culture, and traditions. The majority of people in the Bhaktapur district are Hindus, but there are also followers of Buddhism and other faiths.

1.5.2. Land Use and Land Cover Description

As per Thapa Chhetri & Moriwaki (2017), Bhaktapur district has clearly seen a growth in the built-up area (1989-2015). The built-up area expanded from 1.8 to 24.0 percent between 1988 and 2015. The rate of urbanization was particularly rapid between 2010 and 2015. 12.9 percent of the district as a whole became a built-up area in just five years. Bhaktapur consequently became a well-liked location to relocate as the district's built-up area rose dramatically from 1990 to 2010 (by 22.61%), or by 52.47 percent, reaching 34.15 sq.km.(Wang et al., 2020).

2. Chapter-2: Methodology

2.1. Introduction

This chapter focuses on the methodology employed in the current study, which includes data collection, choosing the best satellite images, pre-processing, and processing of images, as well as components like geometric and radiometric correction, supervised classification, accuracy assessment and comparative analysis.

2.2. Data

Primarily, Seintiel-1 (S-1) level-1 Ground Range Detected (GRD) and Sentinel-2A level-2A data has been used in the study. Both the data products are a part of satellite mission operated by the European Space Agency (ESA) as part of the Copernicus program. Apart from two imageries, other administrative datasets from Survey Department (SD) and Shuttle Radar Topography Mission (SRTM) Digital Elevation Model from NASA, the National Geospatial-Intelligence Agency (NGA), and the German Aerospace Center (DLR) are used for the study.

To integrate Sentinel-2 (S-2) images with S-1 images, a dataset has been selected where each S-2 image has a corresponding S-1 image with the same sensing date. When this was not possible, the similar S-1 image with a 7-day window around the S-2 image's sensing date was used. Based on the target area's features, which normally don't change on a weekly basis, the number of days has been decided. This applies to other scenarios except for the harvesting period.

Table 2. 1: Datasets and its description used for the study

S.no	Descriptions	Sensor type	Data type	Source	Band information	Resolution (spatial, temporal)
1	Administrative boundaries	N/A	Vector	Survey Department	N/A	N/A, N/A
2	Sentinel-1 level-1 Ground Range Detected	C-band Radar	Raster	Copernicus, ESA	VV+VH	5 m x 20 m, 6 days

3	Sentinel-2A Level-1C	Optical	Raster	Copernicus, European Space Agency (ESA)	(490–2190) nm	13 bands at 10 m, 20 m and 60 m, 5 days
4	Shuttle Radar Topography Mission Digital Elevation Model (DEM)	C/X-band Radar	Raster	NASA	DEM	30 m, N/A

2.2.1. Sentinel-1 level-1 GRD

EOS (2021) describes, Sentinel-1 (S-1) is a spacecraft with a core frequency of 5.405 GHz that is intended to observe the Earth in C-band with a 1 dB radiometric precision. A SAR sensor on the satellite allows for imaging in all lighting conditions and at any time of day. Level-1 GRD is the most fundamental and often used data output of S-1 SAR data. It provides concentrated, calibrated SAR data that has been projected onto the ground range using a straightforward range doppler technique. The data is in slant-range geometry. Moreover, depending on the operational mode, the spatial resolution of the S-1 Level-1 GRD product ranges from 5 meters to 20 meters for single-polarization (HH or VV) and dual-polarization (HH+HV or VV+VH) modes. The data is distributed using the Committee on Earth Observation Satellites (CEOS) SAR data product format, which ensures interoperability and compatibility with other SAR data sources.

2.2.2. Sentinel-2A Level-2A

The Sentinel-2A level-1C data products, which have undergone atmospheric correction and radiometric calibration, are used to create the Sentinel-2A level-2A data products (Drusch et al., 2012). This product is referred to as mission analysis ready data (ARD), which means that it doesn't require any additional processing before being used in applications. Processing also includes providing surface reflectance values and removing any remaining atmospheric effects. This process, known as atmospheric correction, accounts for how the Earth's Atmosphere affects the incoming light.

The atmospheric correction technique in Sentinel-2A level-2A makes use of the 'Sen2Cor' algorithm, which is based on the atmospheric correction methods used for the Medium Resolution Imaging Spectrometer (MERIS) and Ocean and Land Color Instrument (OLCI) sensors on board the Environmental Satellite (ENVISAT) and Sentinel-3 satellites, respectively. The 'Sen2Cor' method uses the Level-1C data products as input and produces Level-2A products in units of surface reflectance that have been corrected for atmospheric effects like aerosol scattering and absorption. The sensor specification is listed in the Table 2.2 as given by ESA (2023).

Table 2. 2: Sensor specifications of Sentinel-2

Sentinel-2 bands	**Central wavelength (nm)**	**Bandwidth (nm)**	**Spatial resolution (m)**
Band 1 – Coastal aerosol	442.7	21	60
Band 2 – Blue	492.4	66	10
Band 3 – Green	559.8	36	10
Band 4 – Red	664.6	31	10
Band 5 – Vegetation red edge	704.1	15	20
Band 6 – Vegetation red edge	740.5	15	20
Band 7 – Vegetation red edge	782.8	20	20
Band 8 – NIR	832.8	106	10
Band 8A – Narrow NIR	864.7	21	20
Band 9 – Water vapor	945.1	20	60
Band 10 – SWIR – Cirrus	1373.5	31	60
Band 11 – SWIR	1613.7	91	20
Band 12 – SWIR	2202.4	175	20

2.2.3. Administrative Boundaries

The province, district, and local unit boundaries from the spatial data were used to carry out the study. These boundaries are used for cartographical mapping and GIS operations. To clip the spatial data to the study area for a more thorough analysis, the district boundary is used. By doing this, it is ensured that the analysis only considers factors found inside the study area's boundaries and that no irrelevant places are considered outside of it.

2.2.4. Shuttle Radar Topography Mission Digital Elevation Model

The Shuttle Radar Topography Mission (SRTM) 30 m Digital Elevation Model (DEM) offers accurate elevation data for the land surface of the Earth. It was created as a result of a NASA research that used a radar device to collect elevation data during an 11-day trip in 2000. Each pixel in a 30-meter grid has elevation data in SRTM. Between 56 degrees south latitude and 60 degrees north latitude, it covers the whole geographical surface of the Earth and offers elevation data for both low-lying areas and large mountain ranges.

2.3. Software

All of the study's software are free and open source. QGIS has been utilized for the sample techniques, accuracy assessment and the cartographic mapping. The study uses SNAP for classification purpose.

2.3.1. QGIS

QGIS is a free and open-source GIS program that allows users to create, edit, browse, analyze, and publish geospatial data on a number of operating systems, including Windows, macOS, and Linux (QGIS, 2023). Under the terms of the GNU General Public License, it was created using the Python programming language. Along with a variety of plugins and extensions for more capability, QGIS supports a wide range of vector, raster, and database formats.

2.3.2. Sentinel Application Platform

Sentinel Application Platform (SNAP) is an open-source software platform developed by the European Space Agency (ESA) for processing and interpreting satellite data. The SNAP software platform allows users to access, analyze, and visualize the massive amounts of data collected by the Sentinel satellites. In addition to a variety of tools and algorithms for image calibration, data merging, and data visualization, it also offers tools and methods for processing optical and radar data. SNAP is distributed with the GNU General Public License and is free to download and use.

2.4. Methodological Approach

Figure 2. 1 shows the overall working methodology of the study. The workflow starts with acquisition of images, classifies the image using random forest classification and finally assess the classification using the accuracy assessment measures.

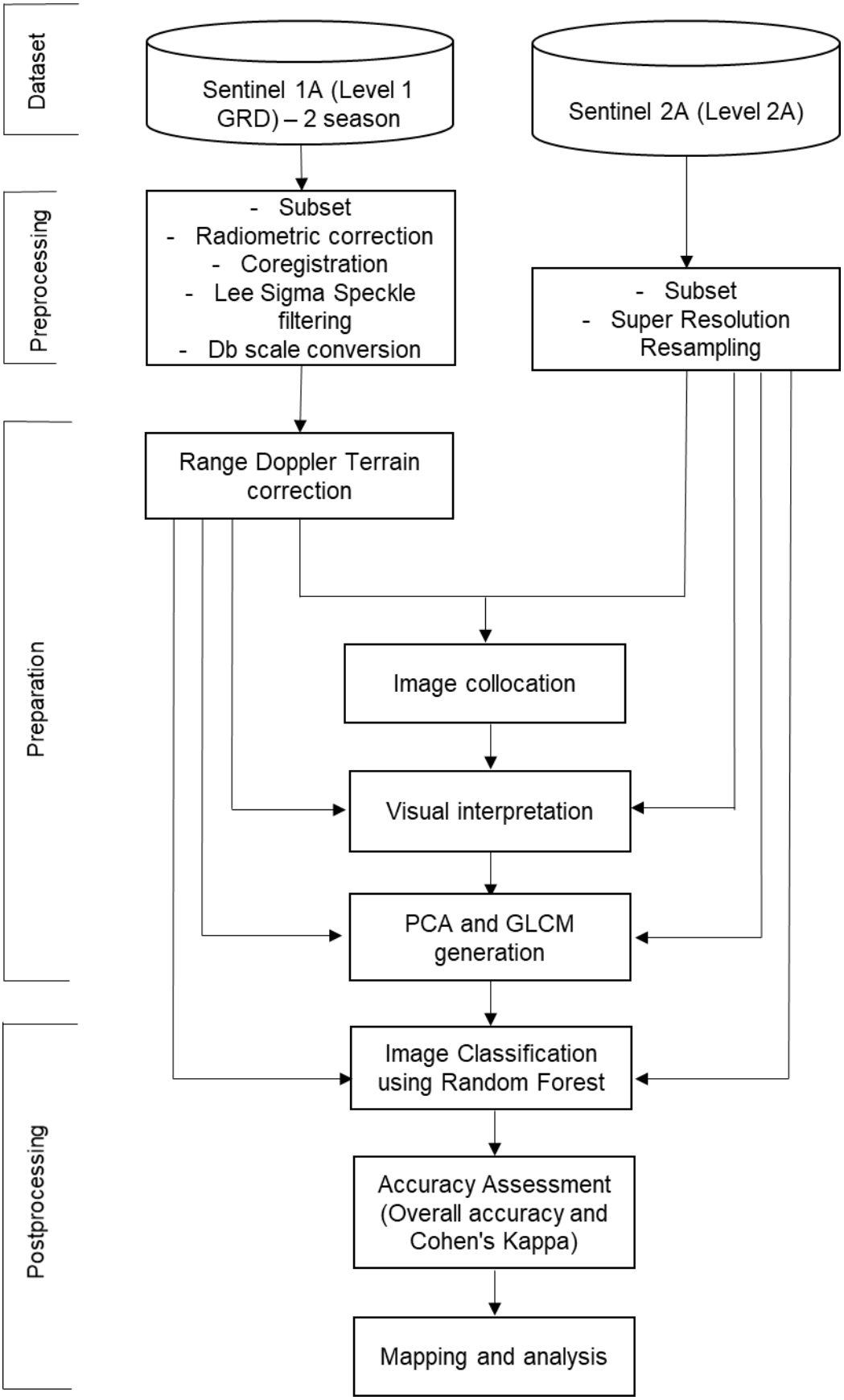

Figure 2. 1: Overall methodological approach of the study

2.4.1. Dataset Acquisition

Sentinel-1 (S-1) and Sentinel-2 (S-2) satellite imageries are downloaded from the Open Access Hub. Open Access Hub is an ESA's platform for the download of satellite data, primarily data from the Sentinel missions as part of the Copernicus program. Administrative boundaries are acquired from the Survey Department, Nepal and SRTM through the SNAP software. All downloaded dataset is free and available after user registration.

While downloading S-1 from the Open Access Hub, following parameters were selected:

- Satellite platform is (Sentinel-1A)
- Product type is GRD: Given that they were projected by the ground range. Backscatter data is sufficient for classification despite the loss of phase data.
- Polarization is VV+VH: VV+VH polarization is frequently chosen for LULC classification because it offers supplementary data on surface characteristics and materials. While VH polarization is sensitive to the moisture content and dielectric constant of the surfaces, such as water, fallow land, and urban areas, VV polarization is sensitive to the roughness and texture of the surface, such as vegetation.
- Sensor mode is Interferometric Wide (IW): Since it is the S-1 satellite's primary and default operational mode over land, IW mode is chosen.

In order to coregister the images, the track number for each is 121. Two images taken at separate points in time or from different tracks will have various sensor orientations and positions, and as a result, different geometric distortions. It is crucial to use images collected from the same track number for coregistration in order to reduce these differences. The orbit number for image or December and June are 43768 and 46043 respectively.

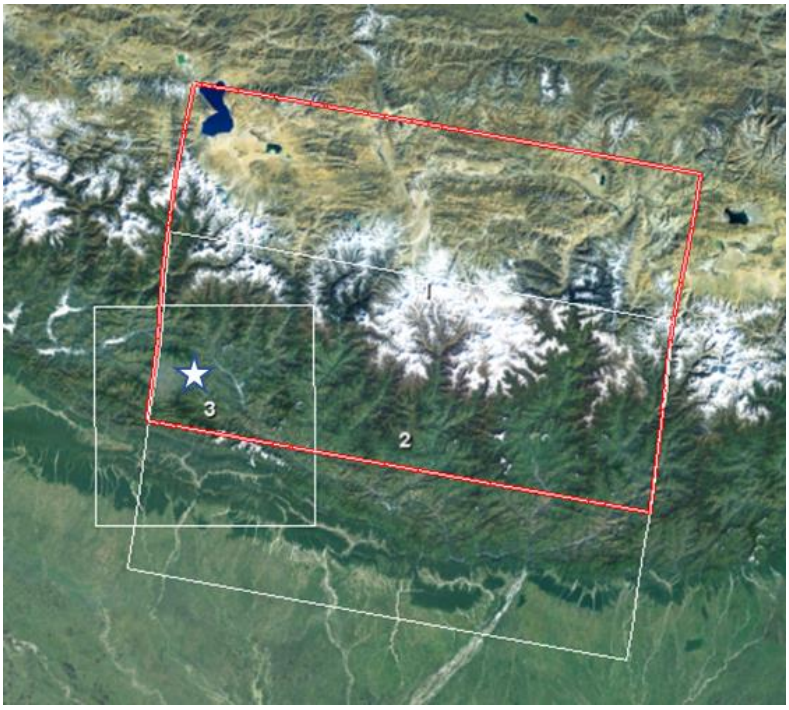

Figure 2. 2: Sentinel-1 image of 25 Nov 2022 (1), Sentinel-1 image of 22 June 2022 (2), Sentinel-2 image of 1 December 2022 (3) and the location where Bhaktapur district is located (star).

Figure 2. 2 is the bounds of downloaded data from the ESA's Copernicus Open Access Hub.

2.5. Preprocessing

Preprocessing is done independently on two images that represent the months of December and June 2022, which are then coregister in the subsequent step. The coverage percentages of the main LULC classes, such as water, fallow land, agriculture, forest, and urban fluctuate throughout two seasons. Trees lose their leaves between November (late autumn) and December (early winter), and the ground's vegetation is in a dormant stage, whereas in June (during the monsoon), both the trees and the ground's vegetation are actively growing. On fallow land, which isn't used for agriculture in November, paddy fields are grown in June in some area. Similar adjustments can be noted for all LULC classes.

2.5.1. Preprocessing of Sentinel-1 Image

i. Subset

A subset is smaller and cropped portion of a larger image. The general steps for subset include selecting and extracting a specific area of interest from an image in order to focus on features or details of interest. The geographic bounds of the subset for the study are north latitude (27.735), west longitude (85.343), south latitude (27.613), and east longitude (85.537).

ii. Radiometric Calibration

Schmidt et al. (2020) explains, radiometric calibration adjusts a physical attribute to the observed pixel intensity. Further, the relationship is developed during calibration for the entire backscatter range, ranging from low image power (near noise) to strong reflections (below saturation). The observed radar backscatter for the S-1 SAR satellite constellation is validated over a broad backscatter range utilizing various target types based on a suitable radiometric calibration.

Further ESRI (2023) elaborates, SAR calibration aims to produce images whose pixel values can be directly linked to the scene's radar backscatter. Although uncalibrated SAR imagery is adequate for qualitative applications, calibrated SAR images are necessary for SAR data's quantitative applications. Radiometric adjustments are typically not included in SAR data processing, which results in Level 1 images and leaves a sizable amount of radiometric bias. The comparison of SAR images taken with several sensors, or taken from the same sensor at various times, in various modes, or processed by various processors, also requires radiometric correction.

Since images were captured over two different dates, radiometric calibration was used to each image to ensure that pixel values accurately represented the radar backscatter of the reflecting surface.

iii. Coregistration

The accuracy of change detection maps can be impacted by even minor registration errors at the sub-pixel level (Sundaresan et al., 2007). Consequently, coregistration of images is crucial. Coregistration of images is the process of matching up two or more images of the same scene captured by various sensors or at various periods. In order to ensure that the images use the same spatial reference system, which is essential for many remote sensing applications, including change detection and multi-temporal analysis, coregistration is used. Following the radiometric calibration of both images in the study's previous stage, coregistration combines them into a single stack. Even if both images were obtained from the same track (relative orbit), little variations in incidence angle can result in incorrect pixel alignment in some areas of the image. The Coregistration Operator detects and compensates for these variations, resulting in a single output product including both images from November and June with the best geometric overlay feasible.

iv. Speckle Filtering

Speckle in SAR images is a general phenomenon induced by the interaction of out-of-phase waves reflected from an object. The presence of speckle in SAR images reduces the interpretability of the data's features (Dasari et al., 2015).

The presence of speckles in SAR images is a substantial problem in image interpretation and analysis. They can obscure visual characteristics, lower image contrast, and make extracting useful information from the image difficult. Speckles can also degrade the accuracy of image classification, change detection, and other applications that rely on image feature analysis (Lee et al., 1994). Various speckle filtering algorithms are used to lessen the effects of speckle noise in SAR images. The objective of these techniques is to minimize speckle noise while keeping image characteristics and contrast. The Lee sigma speckle filter, Frost filter, Gamma Map filter, and Median filter are all commonly used speckle filters (Lee et al., 1994).

For SAR images, the Lee sigma speckle filter (also used in this study) is a popular speckle filtering technique. Lee invented it in 1980, and it is based on the concept of adaptive filtering

(Jong-Sen Lee et al., 2009). The filter operates by first estimating the local statistics of speckle noise in a SAR image and then filtering the image using a weighted average of the pixel values within a short window. The filter lowers the noise while maintaining the image's borders and details.

Default values provided by the SNAP was used for the speckle filtering represented in Table 2. 1. Figure 2. 3 shows a comparison of an image snippet with and without speckle filtering. Due to the presence of speckles, the image on the left is sharper initially, but the image on the right is smoother after speckle filtering.

Table 2. 1: S-1 speckle filtering parameters

Parameter	**Value**
Filter	Lee sigma
Number of looks	1
Window size	7x7
Sigma	0.9
Target window size	3x3

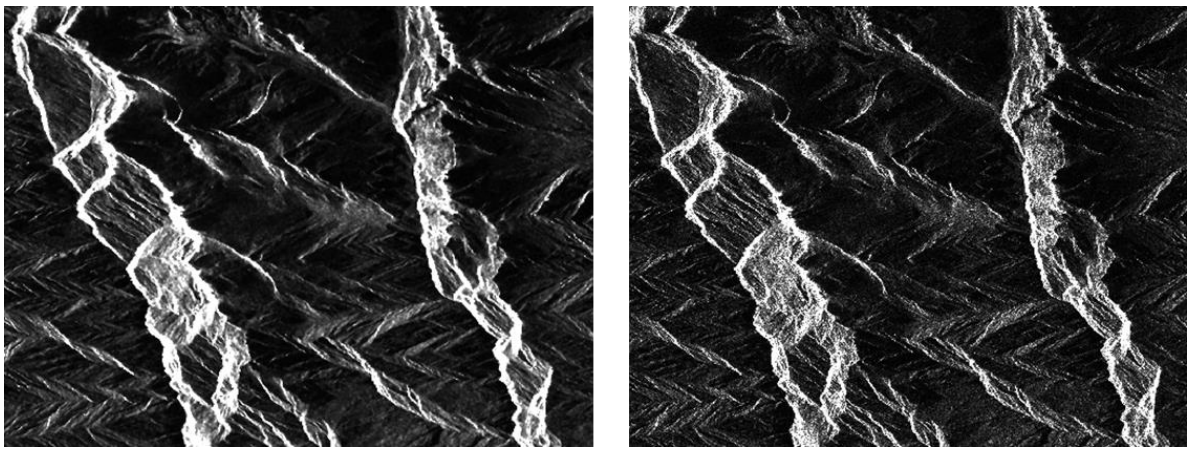

Figure 2. 3: Image before (right) and after (left) speckle filtering of Sentinel-1 image (Nov 2022)

v. Decibel (dB) Scale Conversion

The decibel (dB) scale is commonly used in SAR image processing to express the dynamic range of radar signals. The dB scale is a logarithmic scale that allows us to represent large variations in signal intensity in a more manageable and intuitive way. In SAR, the radar

signal is reflected by the target and returns to the antenna, where it is processed into an image. The strength of the reflected signal varies depending on the properties of the target, such as its roughness, orientation, and composition.

There is an uneven distribution of dark and bright pixels in the image, with more dark than bright pixels. The interpretation of the image is difficult because of this imbalance (as depicted in Figure 2. 4, left). However, a normal distribution of values is produced by transforming the pixel values to a logarithmic scale using the dB scale. As a result, brighter pixel values are moved closer to the mean and darker values are spread across a wider range, increasing contrast (as shown in Figure 2. 4, right).

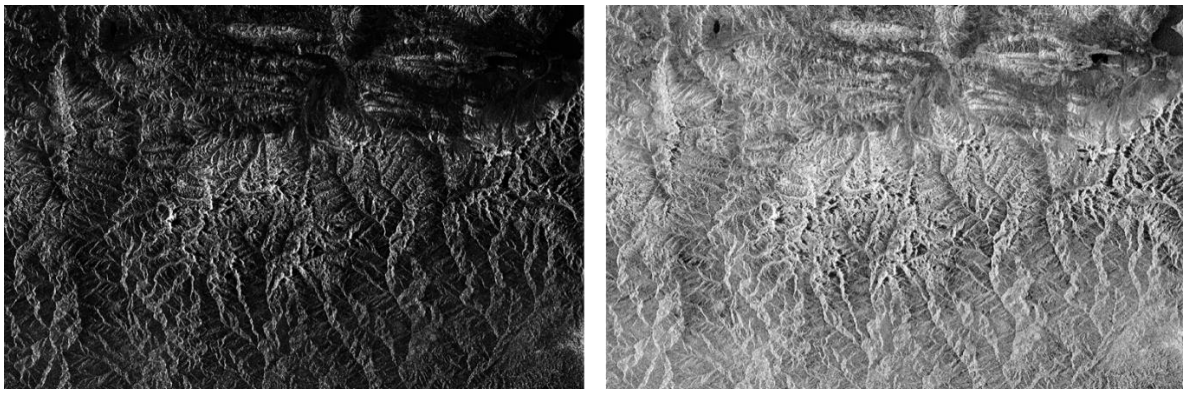

Figure 2. 4: Sigma0 VV before (left) and after (right) conversion to dB scale of Sentinel-1 image

2.5.2. Preprocessing of Sentinel-2 Image

i. Subset

The geographic bounds of the subset for the study are north latitude (27.735), west longitude (85.343), south latitude (27.613), and east longitude (85.537).

ii. Resampling

When it comes to multi-sensor optical images, image resampling is the process of interpolating or decimating the original image pixels in order to change the spatial resolution of the image. When merging or comparing images obtained by various sensors or platforms with varied spatial resolutions, image resampling is necessary in the context of multi-sensor optical images.

Resampling an image may result in some distortion or information loss, particularly if the resolution is raised. To minimize the impact on the quality of the data, it is crucial to carefully analyze the resampling process and settings. For purposes of later analysis and interpretation, it's also critical to record the resampling procedure and maintain track of the information for the original and resampled images, including the pixel size, projection, and coordinate system.

(Lanaras et al., 2018) has described the resampling of S-2 image by Super Resolution (SR). It is a method for enhancing an image's spatial resolution beyond its original resolution by making use of the data present in several low-resolution images of the same scene. The Super Resolution Resampling (SRR) tool in the context of SNAP is a feature that enables users to enhance the resolution of S-2 and other optical satellite images.

To improve the spatial resolution of images, the SRR tool in SNAP employs a machine learning strategy based on a deep neural network. The method works by teaching the neural network the association between low and high resolutions using a set of low- and high-resolution image pairs. The network can be used to upscale new images after it has been trained by predicting the missing high-frequency data. Users can modify the resampling procedure in a number of ways using the SRR tool in SNAP, including the input and output resolutions, the patch size, and the number of iterations.

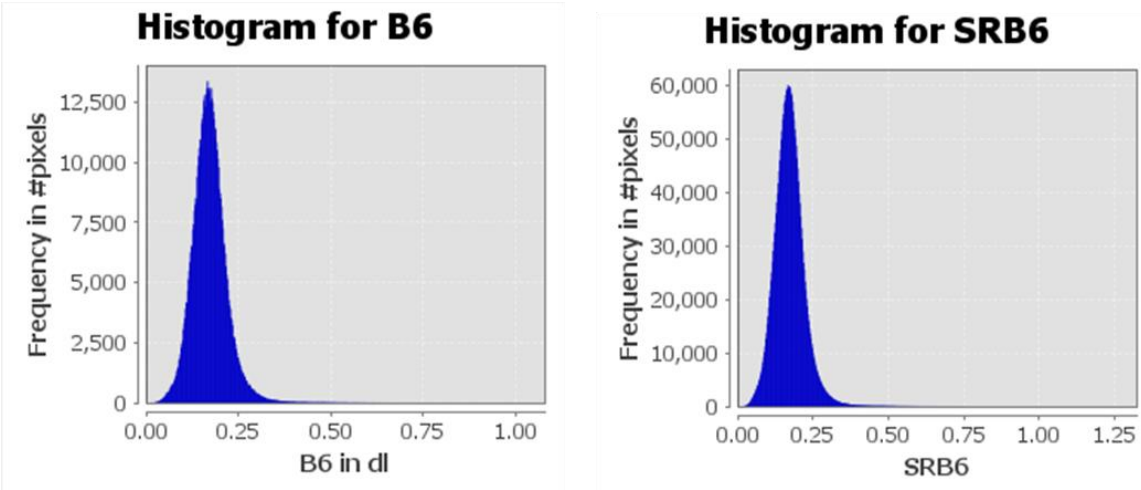

Figure 2. 5: Histogram of Band 6 before (left) and after (right) image resampling of Sentinel-2 image

The frequency of the pixel values is shown to be exactly four times the original one as in Figure 2. 5, comparing the before and after image resampling. The remaining product bands are processed with the same outcome. Map 2.1 which was preprocessed, is the classification-ready map for S-2.

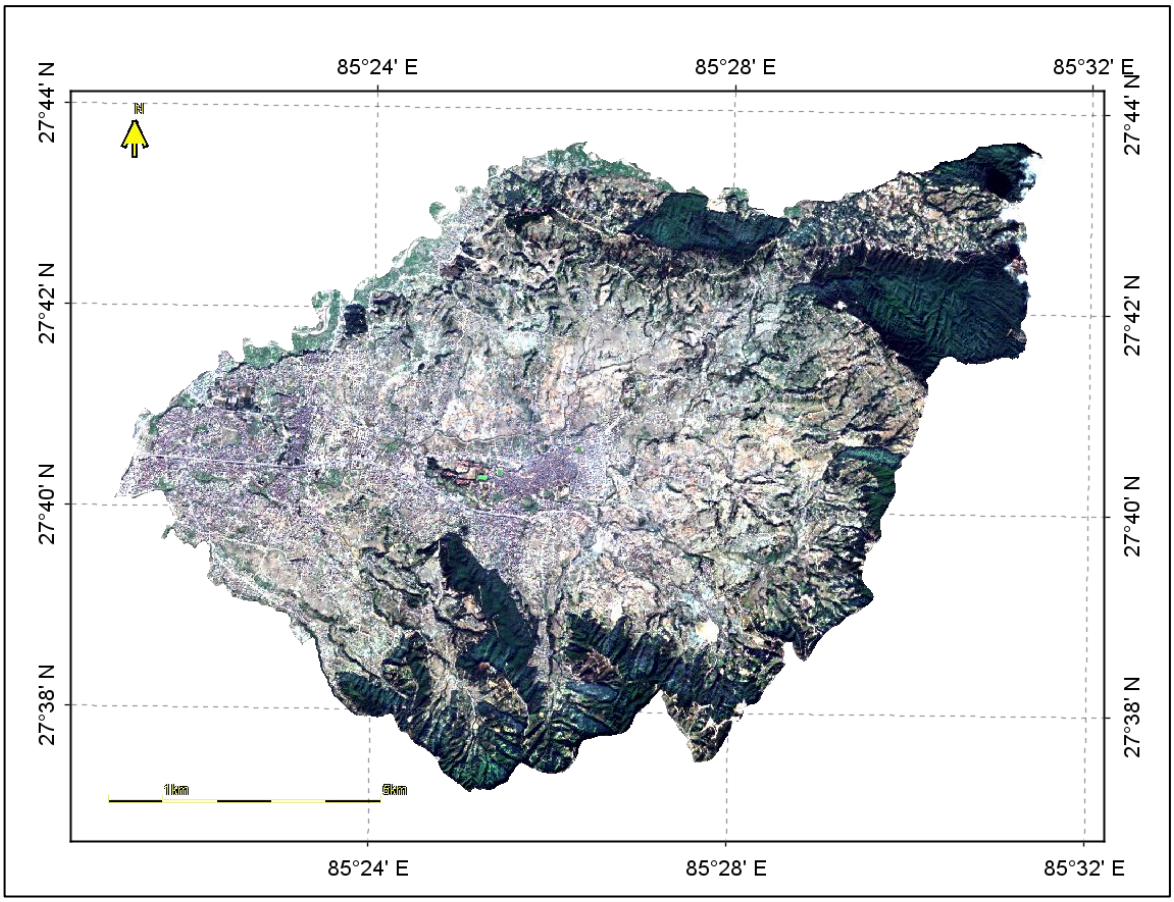

Map 2.1: Classification ready Sentinel-2 image represented in RGB: B4, B3, B2

2.6. Preparation

The preparation is done for S-1 images in following steps:

2.6.1. Preparation of Sentinel-1 image

Through the use of a DEM to precisely project the SAR image onto a map coordinate system, terrain correction corrects these geometric imperfections. In order to correct for distortions brought on by terrain undulations, the DEM gives data about the topography of the Earth. The local incidence angle, or the angle between the SAR beam and the Earth's

surface, is calculated by Terrain Correction specifically using the DEM. Foreshortening, layover, and shadow are adjusted using the local incidence angle.

In order to give range doppler terrain correction with accurate geolocation data, the 1 arc second, 30 m SRTM data is resampled into 10 m for better results. A uniform pixel spacing of 10m x 10m and the map projection WGS 1984 UTM 45N are also used to ensure consistency across the data. Bilinear interpolation is used by the image resampling technique as well as the DEM resampling strategy to improve accuracy. The bilinear interpolation method calculates values between known data points by averaging the four nearest pixel values. This technique allows for the reduction of distortion and noise in the final image product, resulting in a higher-quality outcome that is more suitable for analysis and interpretation.

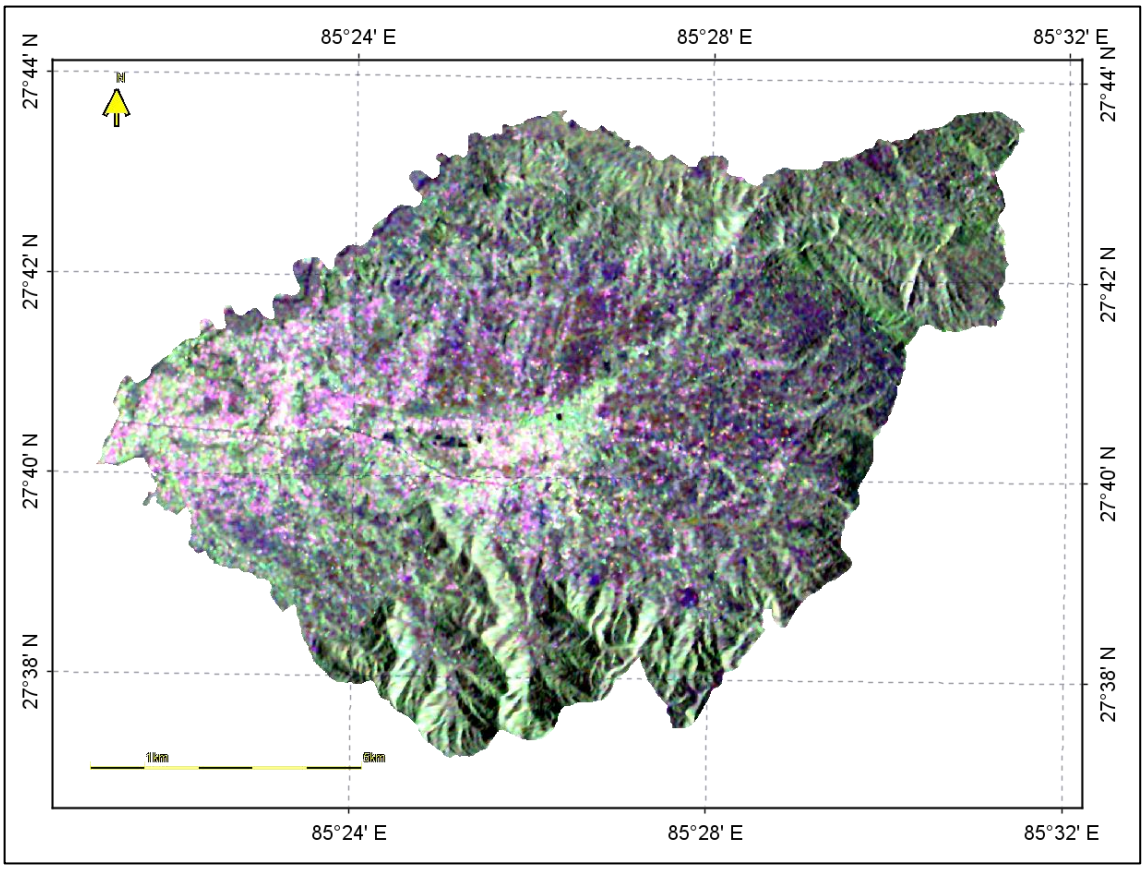

Map 2.2: Classification ready Sentinel-1 image stack of November 2022 and June 2022 represented in RGB: VV(Nov), VH(Nov), VV(Jun)

Map 2.2 is the classification ready coregister S-1 image of November 2022 and June 2022. It is displayed in RGB as VV (Nov), VH (Nov), and VV (Jun).

2.6.2. Image Collocation

The two datasets are stacked as the following step in the LULC classification process, creating a single, analyzed result. Given S-1's high geolocation accuracy following Range Doppler Terrain Correction, it was decided to utilize it as the reference product. This method enables the two datasets to be integrated seamlessly, providing a more accurate and effective analysis.

A master product is the stack of S-1 image, and a slave product is S-2. The technique utilized is bilinear interpolation resampling. Due to its simplicity and capacity to maintain the spatial resolution of the images, bilinear resampling is a used for image collocation between S-1 and S-2 datasets.

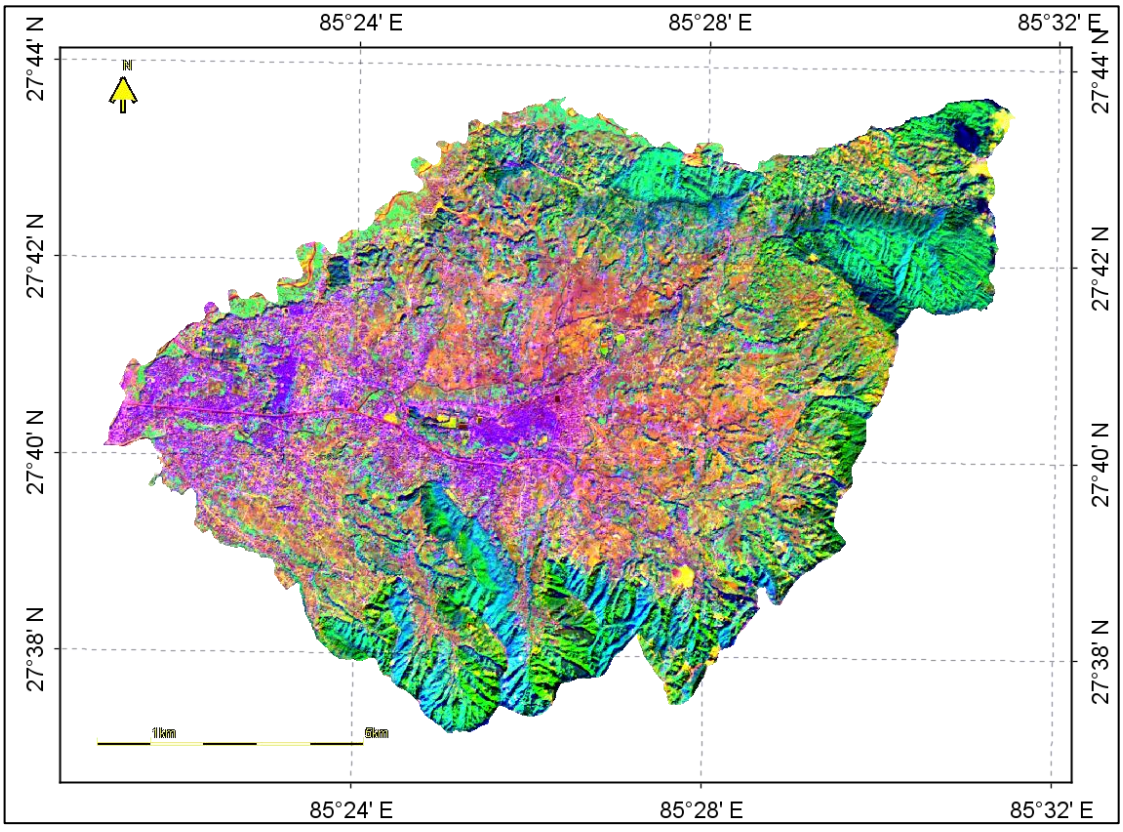

Map 2.3: Classification ready collocated (integrated) image represented in RGB: B4(S2), B8(S2), VV (S1 Nov)

Map 2.3 is the classification ready collocated (integrated) image represented in RGB: B4(S2), B8(S2), VV (S1 Nov).

2.6.3. Visual Interpretation

Visual interpretation of remote sensing images refers to the process of analyzing and extracting information from an image. It is the first step to interpret and image to distinguishing various LULC information by human interpreter. There are six primary elements of visual interpretation are: tone or color, size, shape, texture, shadow and pattern (*Natural Resources Canada*, 2023). The detail is provided in the Table 2. 2.

Table 2. 2: Visual elements definition and examples

Visual element	**Definition**	**Example**
Tone	The relative brightness of the colors present in an image is referred to as tone or color. This component gives a visual clue as to the areas or items in an image.	Green tones in satellite imagery can suggest vegetative cover or forest, while blue tones suggest water bodies.
Size	Size plays a key role in visual interpretation since it tells how big or little the things in the image actually are. This characteristic can aid in identifying large and tiny features in an image and can reveal information about the intended use of the land or property.	Large barren land indicates either urban planning plots or the playground
Shape	Another crucial aspect of visual interpretation is shape. It has to do with the overall shape or organization of certain picture elements. This characteristic can aid in identifying aspects that are man-made versus those that are natural and can shed light on their intended usage or purpose.	The shape of a pond or river can provide important information about its function, such as whether it is a natural or manmade water
Texture	The pattern and frequency of tone variation in specific sections of an image are referred to as texture. This component may contain crucial details about the surface traits of objects or areas within the image.	Smooth and uniform textures suggest manmade surfaces, while irregular and rough textures suggest natural surfaces
Shadow	Shadow is an element that reveals the dimensions and shapes of the items visible in an image. It can help with identification by revealing details about the relative height and profile of various items.	The shadow cast by a vegetation can provide clues about its type – shrub or trees.

Pattern	The spatial arrangement of clearly distinguishable things is referred to as a pattern. This component can give insight on how the image's features are arranged or distributed.	Patterns of roads, buildings, or fields can suggest urban or agricultural land use.

Visual elements in imagery can be examined using remote sensing methods including true and false color (FC) composites, as well as spectral indices like the Soil Adjusted Vegetation Index (SAVI) and Normalized Difference Vegetation Index (NDVI). Usually, distinct spectral bands are assigned to the red, green, and blue color channels of an image display in order to generate band composites. While spectral indices are often generated using information gathered from devices that can detect electromagnetic radiation over a wide range of wavelengths or bands.

The tone of an infrared false-color composite, for instance, can be used to distinguish between various LULC types, with light red possibly representing agricultural lands and dark red possibly representing forest cover. Other band composites and indices, such as SAVI and NDVI, can be interpreted similarly.

While interpreting SAR images can be more difficult, using the appropriate polarization in a color composite and indices can help in recognizing different visual aspects and details. By combining these methods, analysts are better able to comprehend the patterns of LULC in a certain area.

i. Interpretation of Sentinel-1 Image

Sentinel-1 (S-1) is a microwave-operated radar instrument; hence its data does not feature RGB (red, green, and blue) color channels. However, by combining the various polarizations of the radar signal, S-1 data can still be represented in a manner similar to RGB color composites like in Figure 2. 6

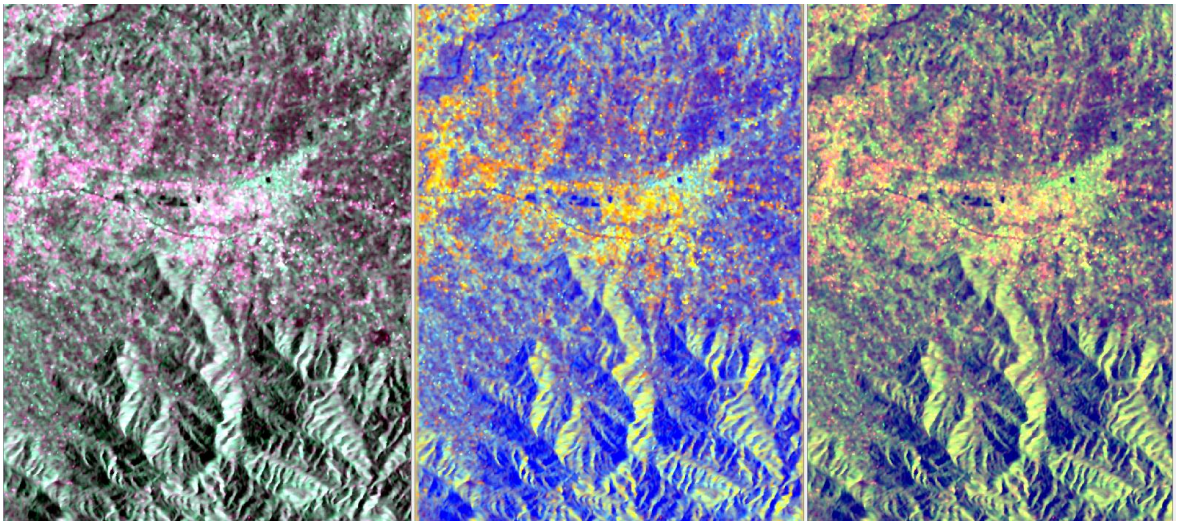

Figure 2. 6: Combinations of polarization as Sentinel-1 FC image (left: RGB-VV, VH, VV+VH, middle: RGB-VV, VH, VV/VH, right: RGB-VV, VH, VH/VV)

ii. Interpretation of Sentinel-2 Image

Along with spectral indices, natural and FC composites can also be used to analyze S-2 data. A three-band composite with multiple uses is shown in Figure 2. 7. Based on their distinctive tones and patterns of construction, urban regions can be recognized in the image on the left. For the objectives of visual interpretation and classification, other composites are equally helpful.

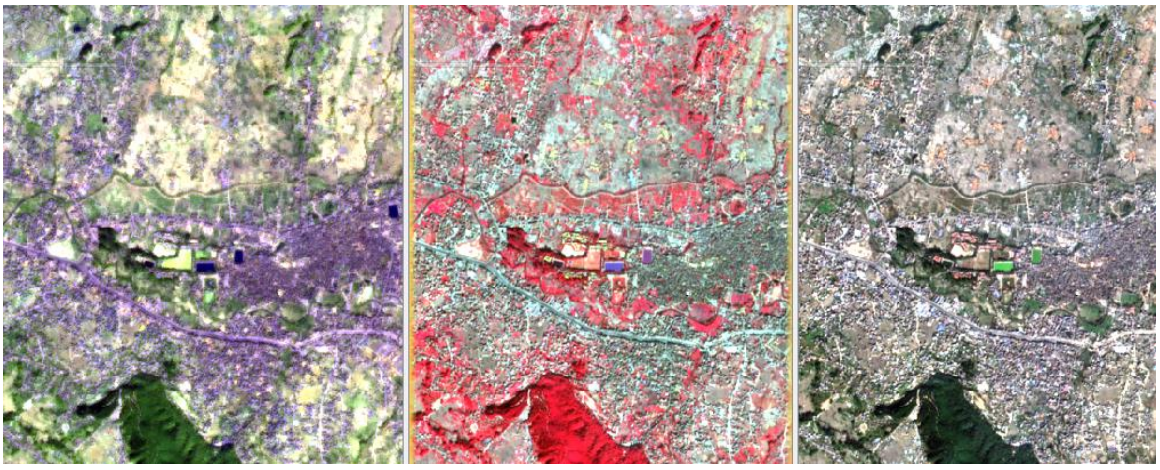

Figure 2. 7: Band composites of S-2 image – false color urban (left), false color infrared (middle), natural color (right)

iii. Interpretation of Integrated Image

It's essential to realize that evaluating integrated images doesn't differ all that much from interpreting individual images. However, bands from both S-1 and S-2 are included in integrated images, which offers complementary information and increase the precision of image interpretation. There is no conventional method for creating composite images or spectral indices to identify characteristics of interest, therefore interpreters must be fully aware of the bands and their relevance. One method is to utilize the S-2 data as the base and then overlay the radar data from the S-1 satellite as a single band to produce a band composite combining data from both satellites.

2.6.4. Dimension Reduction and Texture Generation

Common image processing methods like principal component analysis (PCA) and grey level cooccurrence matrix (GLCM) can be performed individually on S-1 and S-2 images to extract features for classification. There are several things to keep in mind while combining the two images.

The information present in the separate images may already be sufficient for classification purposes, which is one reason why PCA and GLCM are not applied to the integrated image. The integrated image may contain sufficient spectral and textural information to discern between various LULC classes or other interesting features by merging the various bands and polarizations from S-1 and S-2. The integration process may establish correlations or dependencies between the various bands and polarizations, which can impact the findings of these approaches. This is another reason why PCA and GLCM may not be applied to the integrated image. The integration process may alter the distribution of the values used in the GLCM, which assesses the spatial relationship between pixels of the same value, and this may have an impact on the co-occurrence matrix.

vi. Principal Component Analysis

The principal component analysis technique is particularly useful for identifying differences and redundant bands in a stack of bands and restructuring them into principal components, which are new, uncorrelated bands with the highest information richness (Abdi & Williams, 2010). Further Abdi & Williams (2010) describes, a stack of bands may have some bands with identical data, which can cause redundancy. In order to reduce the overall dimensionality of the data while maintaining the majority of its informative richness, PCA can assist in identifying these redundancies and converting them into new uncorrelated bands.

The biggest percentage of variance from the original stack is represented by the first principal component (PC1). This indicates that from the initial data set, PC1 includes the most significant data. Principal components after that express the remaining variation in the data set. The largest percentage of variation from the initial stack is represented by the first PC1. This indicates that PC1 has the most crucial details from the initial data set. Subsequent principal components, such as PC2, PC3, and so forth, express the remaining variation in the data set.

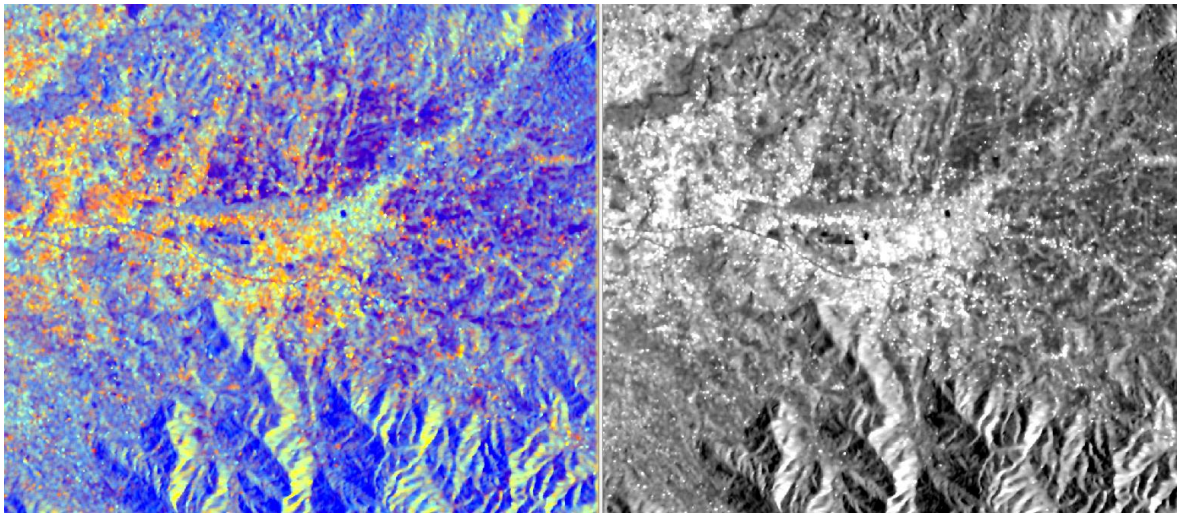

Figure 2. 8: Left: Sentinel-1 RGB (VV (Nov), VH (Nov), VV/VH (Nov)), Right: Principal Component 1 of Sentienl-1 stack

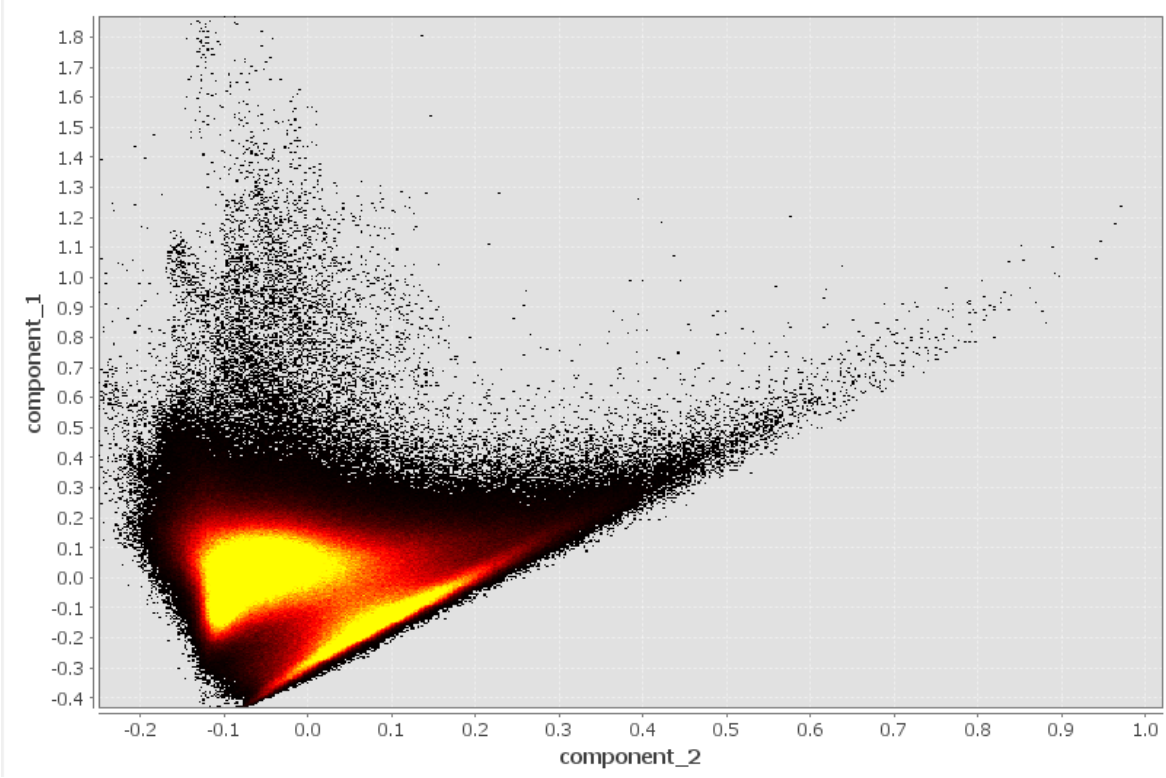

Figure 2. 9: Scatter plot of first and second principal component of Sentinel-2 image

As in Figure 2. 8 left image shows the RGB band composite of S-1 image which helped to identify the vegetation while the right image is the PC1 of S-1 image. The PCA's first component can assist in locating the images' defining characteristics and highlighting regions of change. A pattern or anomaly that may not be seen in the original images can be revealed by the first component, which often indicates the most significant change in the data. Further illustration is demonstrated by the graph between principal components in Figure 2. 9.

vii. Generation of Grey Level Cooccurrence Matrix

The grey level cooccurrence matrix (GLCM) indicates how often different combinations of grey levels occur in a given image (Beliakov et al., 2008). It is a symmetric and square matrix with each element {i, j} indicating the probability of a grey level i, neighboring a grey level j in a given direction. Due to the fact that the majority of them only have a small number of bands, they are particularly well-liked for SAR products (single or dual polarization). Image textures are a means to extend the number of input bands because image

classifications based on a one- or two-dimensional feature space frequently do not produce the requisite accuracies. Following GLCM measures (as described in Table 2. 3) are taken into account while preparing textures as per Beliakov et al. (2008)

Table 2. 3: GLCM measures' formula

Parameter	**Formula**	**Description**
Homogeneity	$\text{Homogeneity} = \sum_{i=1}^{N_g}\sum_{j=1}^{N_g}\frac{\mathbf{P}(i,j)}{1+\lvert i-j\rvert}$	The degree of similarity between neighboring pixels in an image is measured by homogeneity. High homogeneity scores suggest areas with a consistent smoothness or texture.
Energy	$\text{Energy} = \sum_{i=1}^{N_g}\sum_{j=1}^{N_g}[\mathbf{P}(i,j)]^2$	The total textural strength of an image is gauged by its energy. Areas with high energy values have a lot of texture or intricacy.
Entropy	$\text{Entropy} = -\sum_{i=1}^{N_g}\sum_{j=1}^{N_g}\mathbf{P}(i,j)\log_2[\mathbf{P}(i,j)]$	A measure of an image's unpredictability or disorder is called entropy. The presence of chaotic or erratic patterns is indicated by high entropy values.
Maximum probability	$\text{Maximum probability} = \max\{P(i,j)\}$	The most frequent pair of gray levels or texture pattern in the image is represented by Largest Probability (Pmax), the maximum value in the GLCM.
Mean	$\mu_i = \sum_{i,j=0}^{N-1} iP_{i,j}\ \mu_j = \sum_{i,j=0}^{N-1} jP_{i,j}$	The mean of all the gray level pairings in the image is represented by the GLCM (Mean), which is the average gray level value of the GLCM.

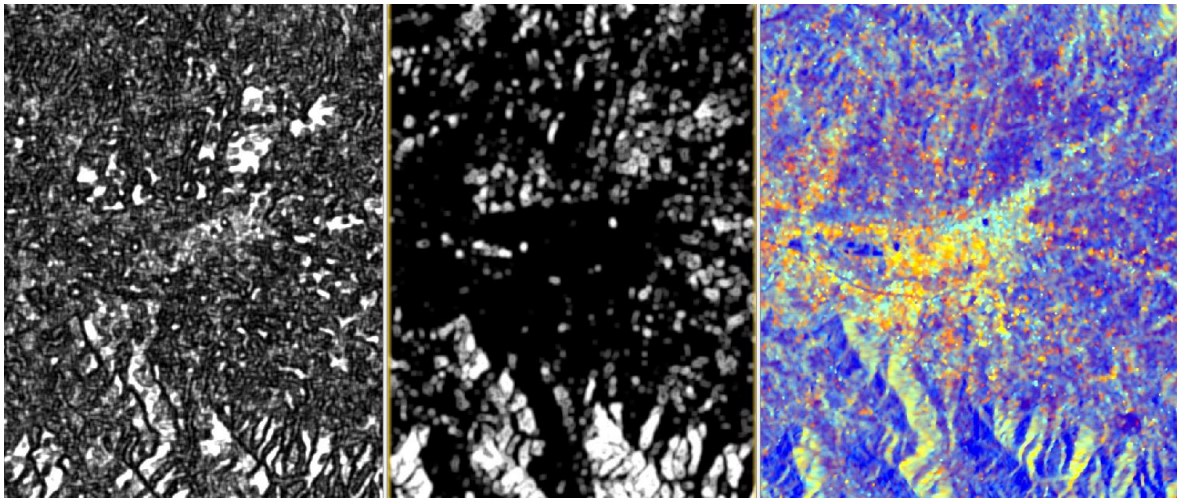

Figure 2. 10: left: Sentinel-1 VH (June) Homogeneity, Middle: Sentinel-1 VV (June) Entropy, right: Sentinel-1 (RGB: VV (Jun), VH (Jun), VV/VH (Jun))

As in Figure 2. 10, the comparison between neighboring pixels in an image is depicted in the left image. High homogeneity denotes regions with consistent smoothness or texture. Entropy is seen in the middle image. The presence of chaotic or erratic patterns is indicated by high entropy values in the right image.

2.7. Postprocessing

2.7.1. Image Classification

The classification stage is essential in the supervised classification process. Here, the algorithm evaluates each pixel's spectral pattern using pre-established decision rules to ascertain the pixel's identification (Lillesand et al., 2015). The stages of supervised classification are also explained by Lillesand et al. (2015). Under supervision, the analyst chooses these samples, or training areas. There are three steps in supervised classification: A LULC class is assigned to each pixel in the image data set during the following stages: (1) training, which involves selecting representative training areas and creating a numerical description of the spectral attributes of each LULC class in the scene; (2) classification; and (3) output, which entails a matrix of interpreted LULC class types.

i. Classification Scheme

Based on the Anderson (1976), LULC classification method for a level one classification and thorough understanding of the topography the classification scheme is developed into five categories: water, barren land, agriculture, and forest. Detail is provided in the Table 2. 4.

Table 2. 4: Land use and land cover classes description

LULC class	Description
Forest	Forest, grassland with shrubs
Agriculture	Agricultural fields and plastic tunnel farming
Urban	Buildings, roads, and concrete constructions which are man-made infrastructures
Fallow land	Places with exposed soil (used by brick factory, uncultivated land, newly developed urban planning plots)
Water body	Ponds, rivers

ii. Digitization of Training Datasets

The indices and band combinations of S-1 and S-2 are used to digitize the training datasets as samples for LULC have been a prerequisite for supervised classification (Lillesand et al., 2015). The training samples (Map 2.4) are manually digitalized utilizing combinations of bands from both the images and spectral features based on classification systems and visual interpretation.

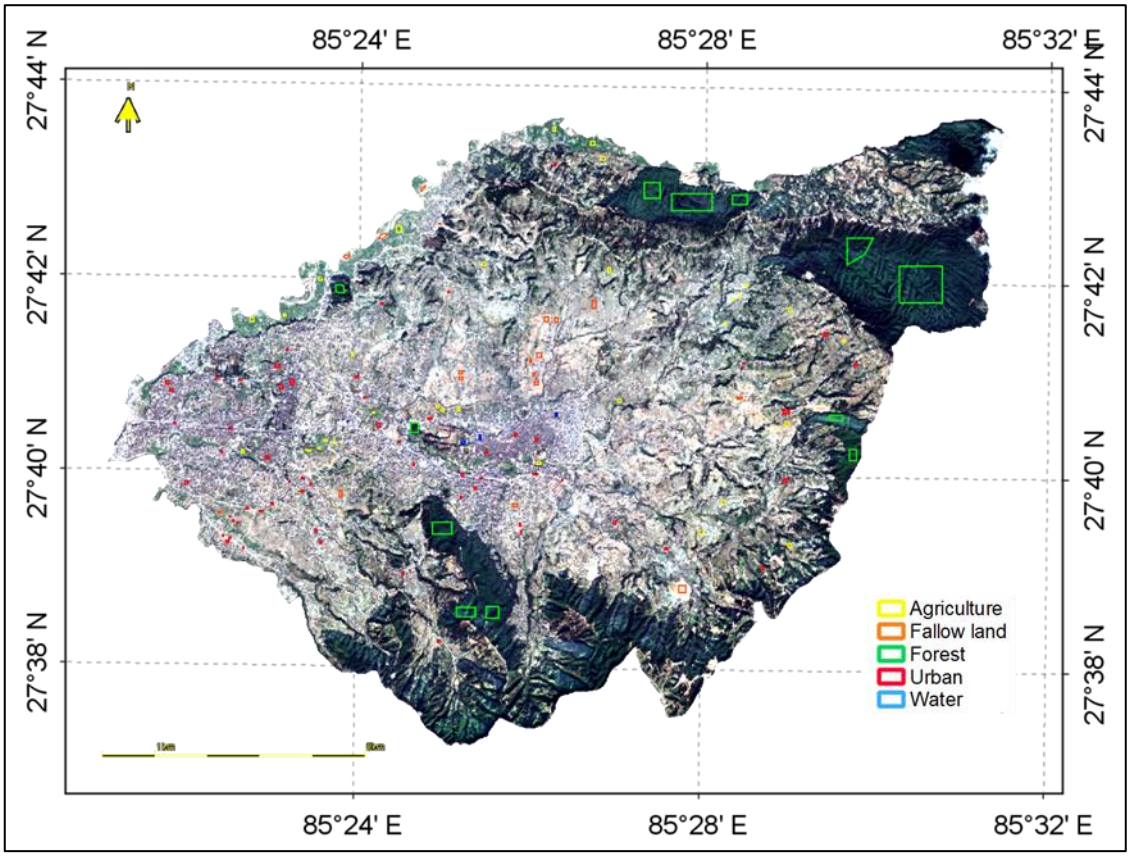

Map 2.4: Digitized training samples, Senitnel-2 natural colors image as base

Table 2. 5: Sample of digitized training sample polygons with false color infrared composite base

Class	Sample 1	Sample 2	Sample 3
Forest	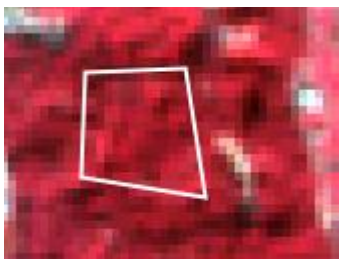		
	Dense forest	Grassland with shrubs	
Agriculture			
	Seasonal cash crops	Tunnel farming	Uncultivated land

Urban	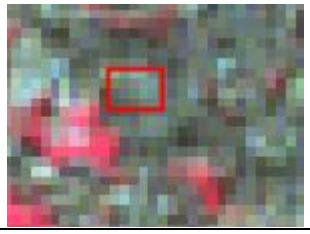		
	settlement	road	
Fallow land	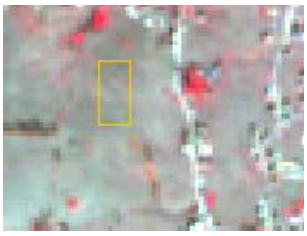		
	Mud extracted land for brick making	River bed	Urban settlement plot
Water body			
	Pond		

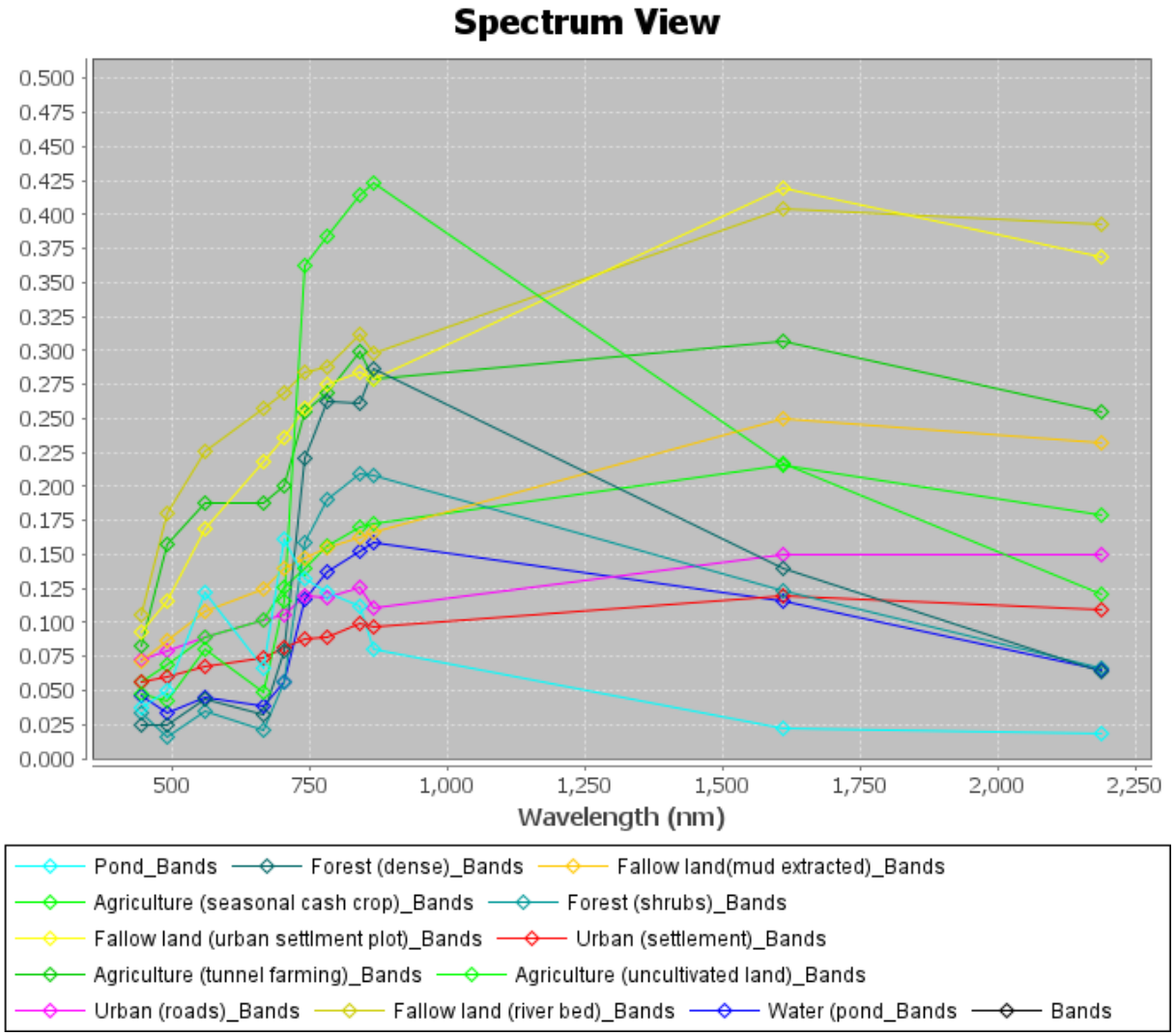

Figure 2. 11: Spectral signatures of training samples

While Table 2. 5 shows the frames of training sample stacked over the FC composite of S-2 image, Figure 2. 11 shows the spectral signatures of the training samples are per class and the sub-classes.

iii. Supervised Classification

In order to create thematic maps, preprocessed satellite imagery was used, and information classes were recovered using supervised classification techniques. The supervised classification was performed in SNAP software. The RF supervised classification method was utilized for analyzing all the image stacks. The training of this method involved digitized training samples for each LULC class, and a set of 5,000 training samples and 50 trees

were established. Out of these 50 trees, the ones that fitted the model were selected and tested.

The classification was performed for both S-1 and S-2 images, either with or without the use of GLCM measures and PCA. An integrated image was also created, and its classification was performed without the use of GLCM measures and PCA. The images and their combination for classification is shown in the Table 2. 6.

Table 2. 6: Image stacks used for classification[1]

Source image	Processed image	Classification stack
Sentinel-1	-	Sentinel-1
	PCA	Sentinel-1, Sentinel-1 PCA
	GLCM	Sentinel-1, Sentinel-1 GLCM
	PCA, GLCM	Sentinel-1, Sentinel-1 PCA and Sentinel-1 GLCM
Sentinel-2	PCA	Sentinel-2
	GLCM	Sentinel-2, Sentinel-2 PCA
	PCA, GLCM	Sentinel-2, Sentinel-2 GLCM
	-	Sentinel-2, Sentinel-2 PCA and Sentinel-2 GLCM
Sentinel-1 and Sentinel-2 integrated	-	Sentinel-1 and Sentinel-2 integrated

2.7.2. Accuracy Assessment

After the classification, it is important to evaluate the accuracy of the results as classification is not complete without the validation (Lillesand et al., 2015). Accuracy assessment plays a vital role in the workflow for detecting LULC changes by verifying the accuracy of classified data. This process helps determine the quality of classification results. To accurately observe LULC changes in a study area, it is necessary to verify the classification results of

1.

[1] PCA: principal component analysis; GLCM: grey level cooccurrence matrix

the datasets and the accuracy should be at least 85 percent for satellite imagery LULC classifications (Anderson, 1976), as is adopted in the study. It is done in three steps:

i. Creation of a Validation Dataset

A validation dataset was produced using stratified random sampling since there is availability of diverse groups (i.e., LULC classes). The strata will be mutually will be exclusive and collectively exhaustive, meaning that every pixel or area in the study area shall belong to one and only one stratum.

Provide an adequate number of samples for each class, even if the class area proportion (*Wi*) is low. The number of samples (*N*) will be calculated as (Olofsson et al., 2014):

$$N=(\sum i=1\ (Wi*Si)/So)^2$$

where:

- Wi = mapped area proportion of class i;
- Si = standard deviation of stratum i;
- So = expected standard deviation of OA;
- c = total number of classes;

The sample size for each class is multiplied by 1.5 to make sure that both the best and the most perplexing cases are taken into account during the verification process. In order to ensure that they are sufficiently validated for higher accuracy, classes with low percentage coverage are also increased by a factor of 3. It is represented in the Map 2.5.

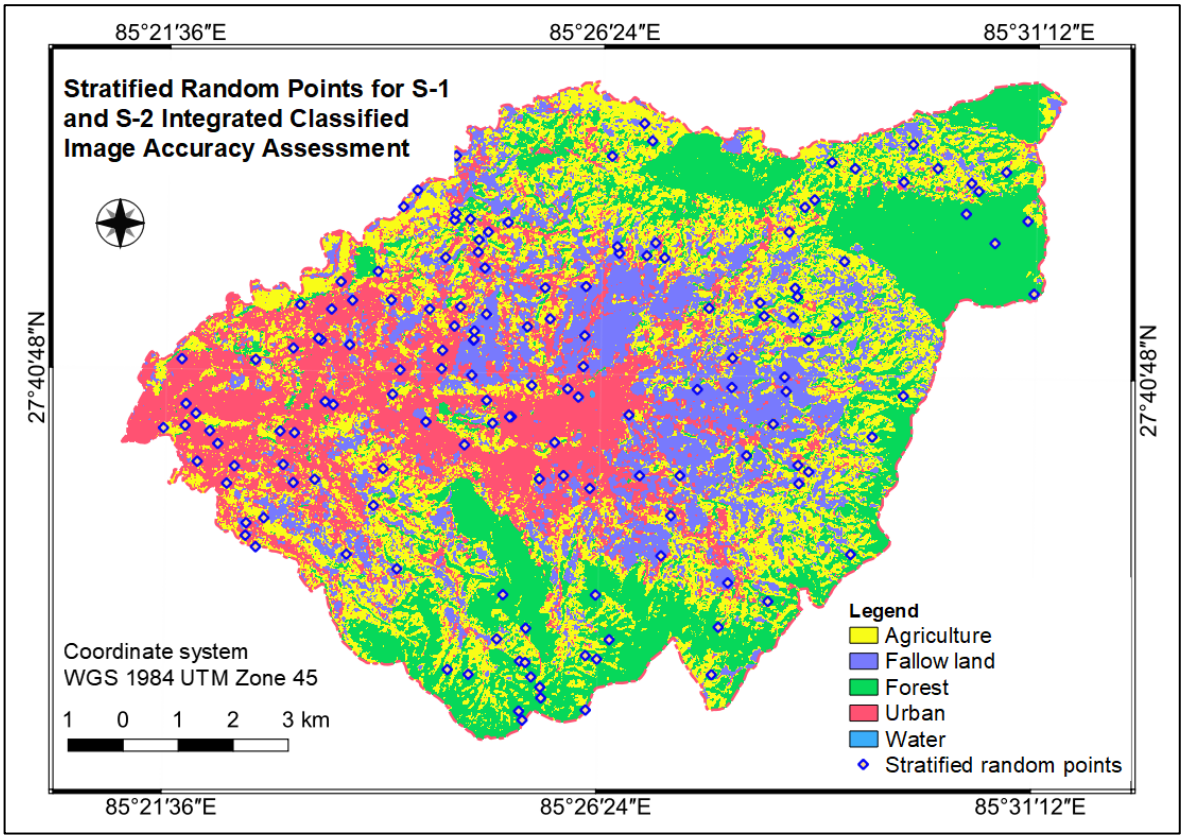

Map 2.5: Stratified random points for Sentinel-1 and Sentinel-2 Integrated Classified image accuracy assessment

ii. Verification of the Validation Dataset

A two-step approach is used to validate the dataset. First, the verification dataset was placed on top of the satellite maps from Google and Bing. Since (Uddin et al., 2015) publication is the latest LULC maps in Nepal, and since the most recent datasets to reflect the change in study period are not publicly accessible, Google and Bing satellite images are used for the procedure. Second extracting the confused points and having field surveys that helped to identified ground truth of the image. A more thorough and comprehensive evaluation of the classification results was provided by on-site field surveys, while the utilization of high-resolution imagery from Google, Bing, and ESRI Imageries gave an objective way to confirm the accuracy of the results. The main benefit is that Google Earth contains an image from November 22, 2022, which corresponds to the acquisition dates of the two images and is therefore in the same season.

While the confusing pixels are confirmed using ground surveys, the certain results are confirmed through satellite images.

iii. Statistical Analysis

In order to compare the accuracy of the classification results, statistical measures like overall accuracy (OA) and Cohen's Kappa were used. The OA is a measurement of the total proportion of properly categorized points in the validation dataset, whereas the Cohen's Kappa is a statistical indicator of agreement between the observed and anticipated classification results (Lillesand et al., 2015). Additionally, 95 percent confidence intervals were employed to assess the importance of variations in the classification results' accuracy. The area-based error matrix is used to generate these statistics specifically, and each element in the matrix reflects the estimated area fraction of each class.

2.7.3. Mapping and Analysis

After classifying the data and evaluating its accuracy, the following phase is mapping and analyzing the combined usage of S-1 and S-2 for LULC analysis, together with GLCM and PCA, in order to determine whether the hypotheses posed by the objectives and research questions can be supported. This chapter is essential for analyzing the classified images from all S-1 and S-2 stacks, integrating them, and visually interpreting them to establish the best-case scenario, worst-case scenario, and dependability in each class of classified image. Although the classification parameters are the same for all forms of images stacks, the interpretation of the findings may vary depending on the particular type of image chosen as the classifications are influenced by the band and polarization choices.

For a thorough investigation of the identified images, this part can be further divided into two sub-sections. The visual interpretation of the classified images is covered in the first subsection. In this step, the classified images are examined to evaluate their accuracy and quality. The ideal situation, where the classification accurately captures the LULC

characteristics of the study area, will be seen in this subsection. The worst-case situation, on the other hand, is when the classification outcomes are flawed and there is a substantial discrepancy between the classified image and the ground truth information. This subsection additionally evaluates each classified image's classes accuracies. Low accuracy percentage imply that the classification may not be accurate, whereas high accuracy percentage show that the classification results are highly accurate.

The second subsection of the mapping and analysis section compares the outcomes of image stacks. In this stage, the variations between the classified images from the S-1 and S-2 data, and their integration will be looked upon. Assessing the accuracy and quality of the classified images based on various factors, including spectral resolution, temporal resolution, and spatial resolution, will be a part of the comparison. The results from the subsection can be used to assess how well S-1 and S-2 work together while performing LULC analysis.

3. Chapter-3: Results and Discussion

This chapter presents the accuracy assessed land use and land cover (LULC) maps prepared using random forest (RF) for Sentinel-1 (S-1), Sentinel-2 (S-2), it's PCA and GLCM combination and S1 and S-2 integration.

3.1. Visual Interpretation

Setninel-1's representation in a false color (FC) composite makes it difficult to interpret visually. S-1 imagery interpretation is more complex compared to optical imagery, especially in places with steep terrain where radar signals can be bounced away from the sensor, producing low backscatter or shadows in the image. As shown in Figure 3. 1, these shadowy patches occasionally mimic bodies of water. Water, agricultural, and fallow ground appeared to have low backscattering values. Similar to this, high backscatter caused urban areas and some forest regions to seem brighter in S-1 images, as seen in Figure 3. 1.

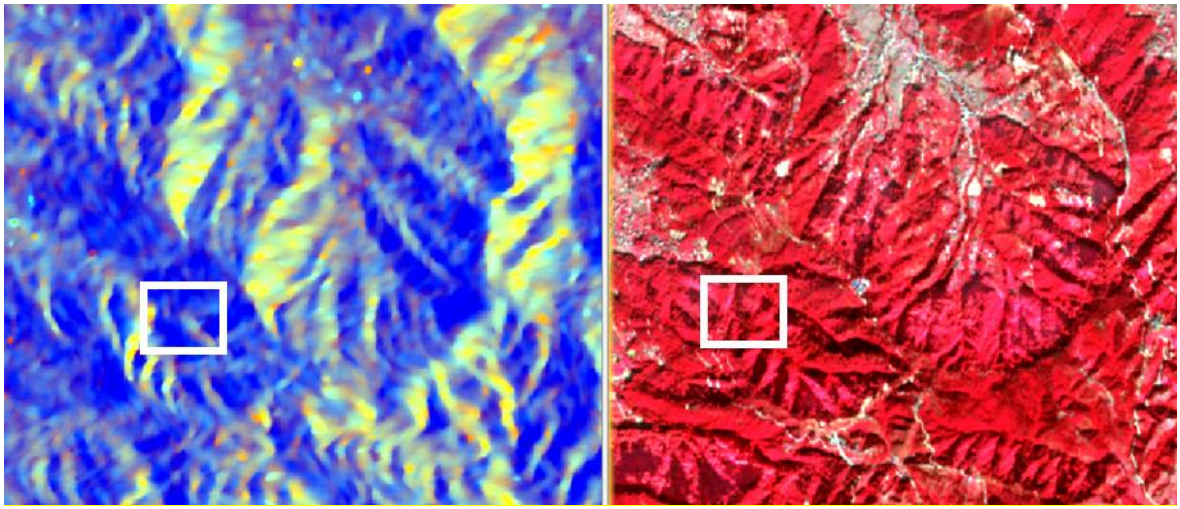

Figure 3. 1: Left: Shadows in the Sentinel-1, Right: false color composite of Sentinel-2 with forest area

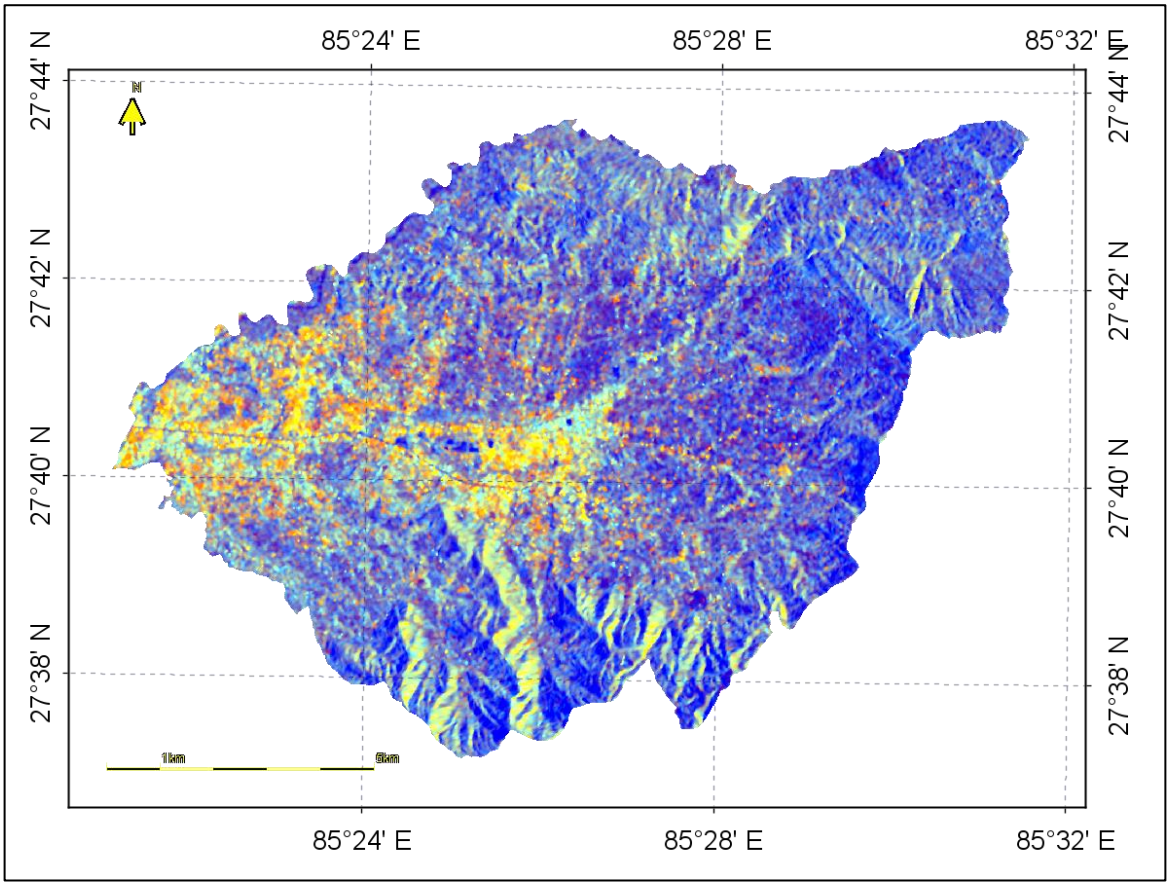

Map 3.1: Sentinel-1 image (RGB: VV (Jun), VH (Jun) and VV/VH (Jun)) that shows varying backscattering in the land use and land cover classes

The generation of both true color and FC composite is possible due to the moderate spatial and high spectral resolution provided by S-2 images. FC composite can be used to determine LULC classes depending on how pixels appear in the image. In Map 3.1, for instance, urban areas appear as light green (settlements) and white (roads), whereas fallow land appears grey, water is seen as dark blue and pink, and vegetation is evident as red. Pixel classes are determined by examining how pixels appear in the FC composite. The possibility for spectral misunderstanding between related classes as well as aspects like the spectral features of various LULC classes must be carefully taken into account in order to accurately classify LULCs.

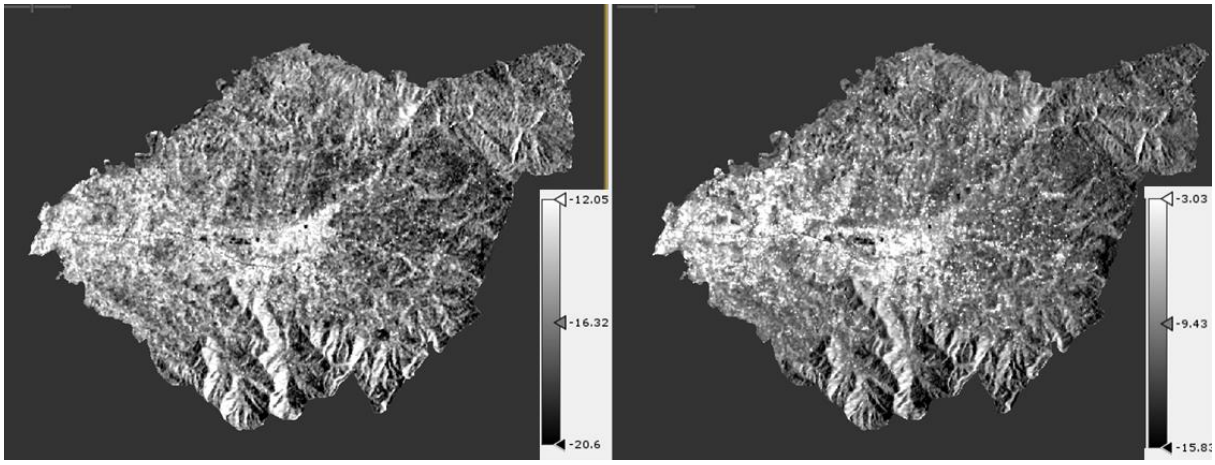

Figure 3. 2: Left: VH polarization Right: VV polarization of image of November Sentinel-1 image

When comparing the two images as in Figure 3. 2. The right image with the representation of the black colors indicates the roughness and texture of the surface of the classes where the vegetation and fallow land are clearly displayed. Given that VH polarization is sensitive to moisture content and dielectric characteristics, the black tones in the left image represent moisture content. With the use of shadow analysis and thresholding, even the most confusing classifications, like agriculture and forests, may be differentiated.

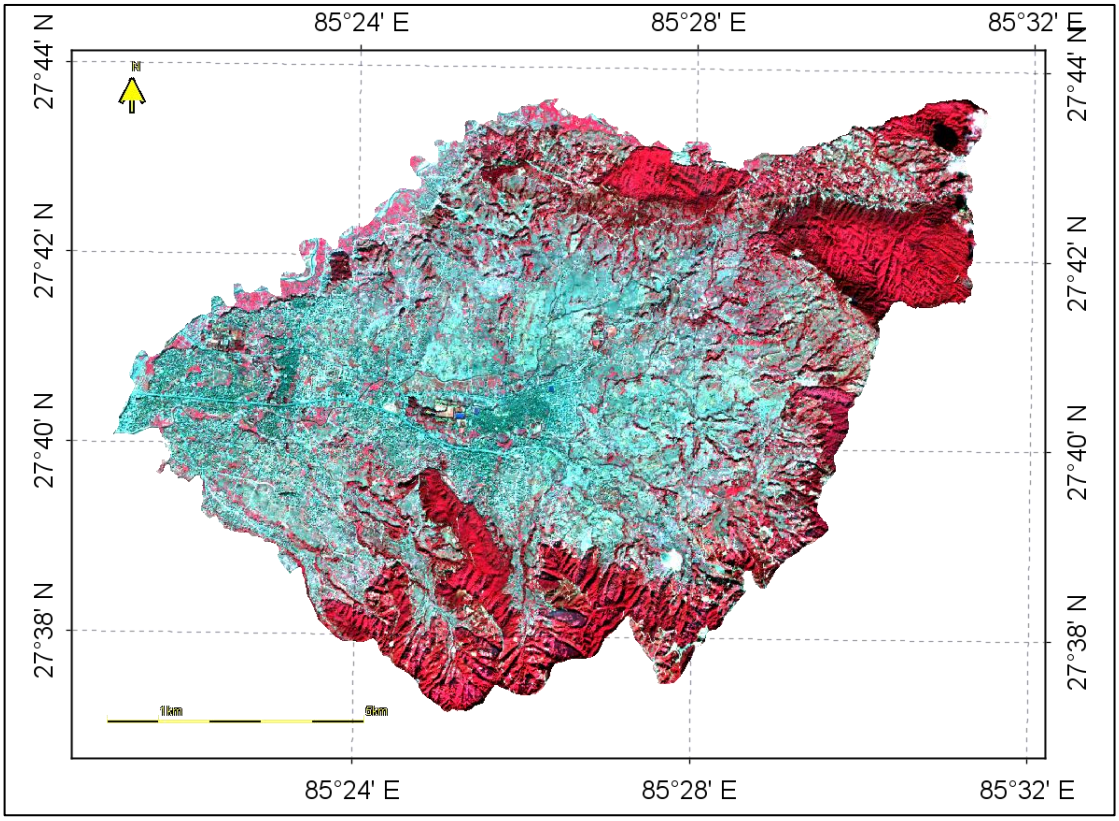

Map 3.2: False color composite map of Sentinel-2 image

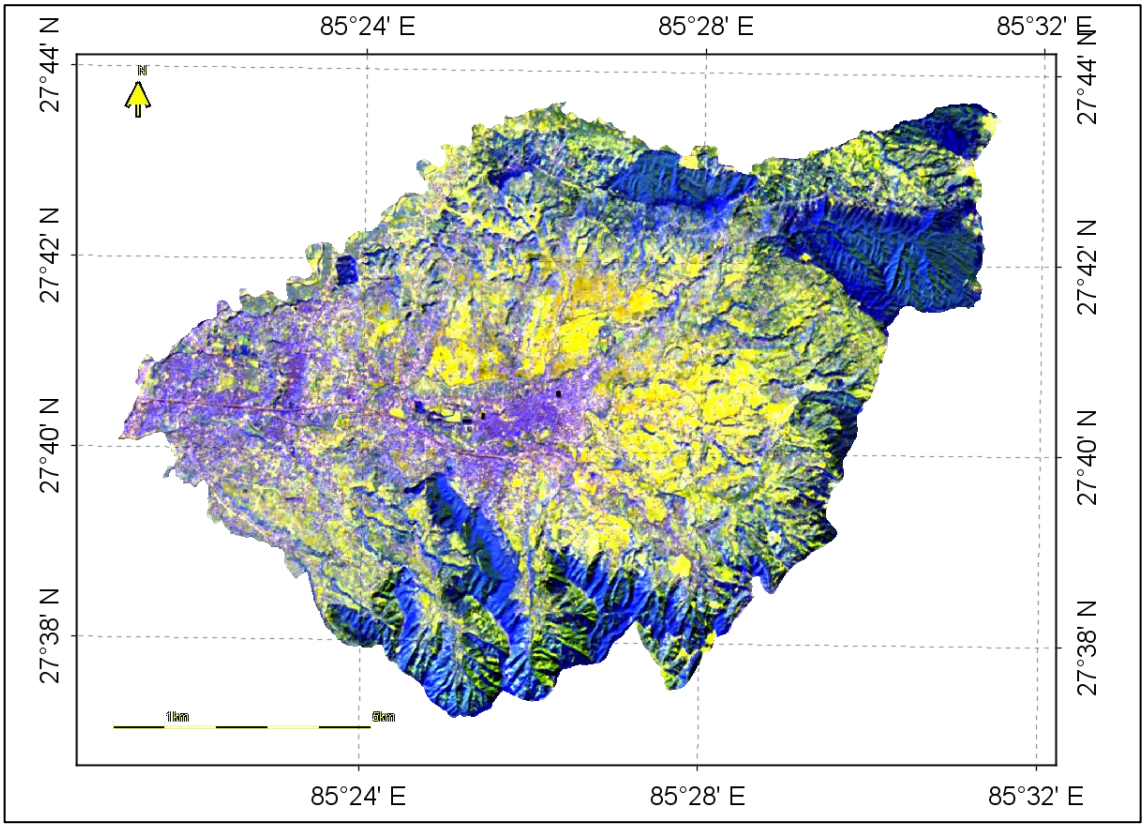

Map 3.3: Sentinel-1 (S-1) and Sentinel-2 (S-2) integrated false color composite image with RGB (B12 (S-2), B11(S-2) and VH Nov (S-1)

Combining S-1 and S-2 imaging can enhance the spatial resolution and facilitate improved change detection, according to earlier studies. Figure 3. 3, which also shows the value of this approach, supports this observation. In particular, the red, green, and blue channels in the image were created using S-2 bands, whereas the S-1 VH polarization data from November was used to create the blue channel. The image successfully distinguishes between several LULC classes, emphasizing the advantages of combining data from S-1 and S-2 to improve resolution and change detection.

3.2. Classification and Map Statistics

Different classification stacks' findings have revealed variances in the LULC classes' coverage. In particular, compared to combining S-2 with PCA and GLCM, as well as the combined image of S-1 and S-2, the combination of S-1 with PCA and GLCM has produced distinct findings. In example, compared to previous classification stacks that primarily

identify water and forest classes, the percentage of agriculture, fallow land, and urban classes is much lower in the S-1 and S-2 with PCA and GLCM combination classification stacks. The proportion of LULC class coverage according to the classification stack is shown in Table 3. 1.

Table 3. 1: Classification stack and it's land use and land cover class area coverage

Image	Processed images	Agriculture (%)	Fallow land (%)	Forest (%)	Urban (%)	Water (%)
Sentinel-1	-	11.18%	13.96%	53.32%	20.36%	1.18%
Sentinel-1	GLCM	12.28%	13.33%	49.01%	23.29%	2.08%
Sentinel-1	PCA	9.10%	13.60%	52.77%	22.47%	2.06%
Sentinel-1	PCA, GLCM	12.06%	12.44%	51.03%	22.31%	2.16%
Sentinel-2	-	31.92%	20.39%	24.71%	22.95%	0.03%
Sentinel-2	GLCM	37.19%	12.83%	17.61%	31.84%	0.54%
Sentinel-2	PCA	30.62%	20.37%	25.85%	23.14%	0.03%
Sentinel-2	PCA, GLCM	31.77%	14.59%	24.99%	28.62%	0.02%
Sentinel-1 & Sentinel-2	Integrated	30.28%	19.91%	26.69%	23.09%	0.03%

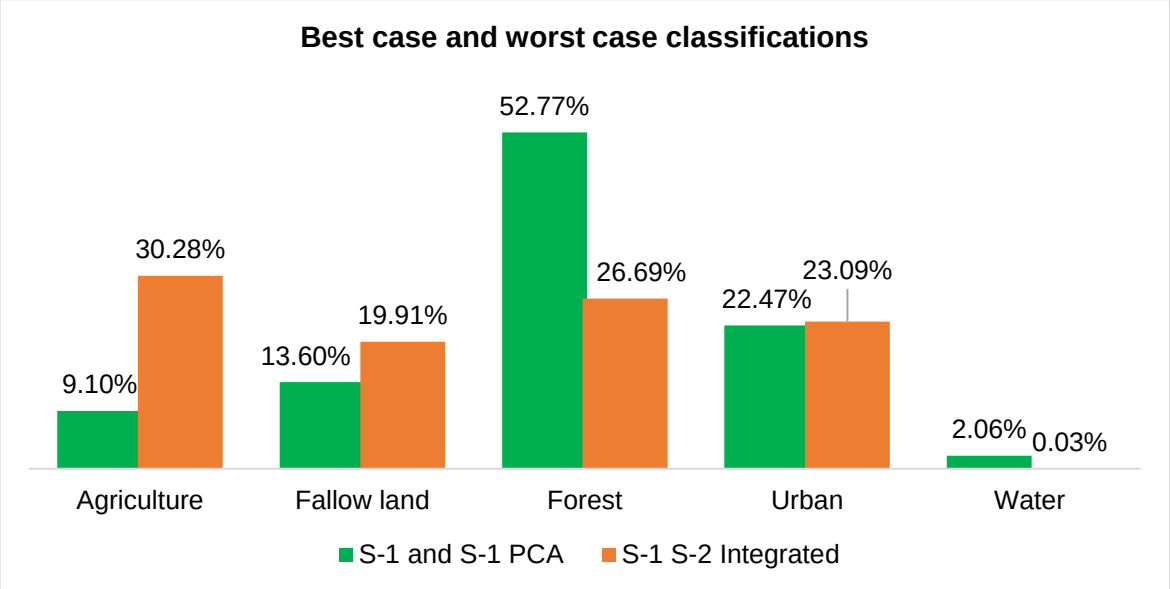

Figure 3. 3: Best case and worst-case classification class distributions

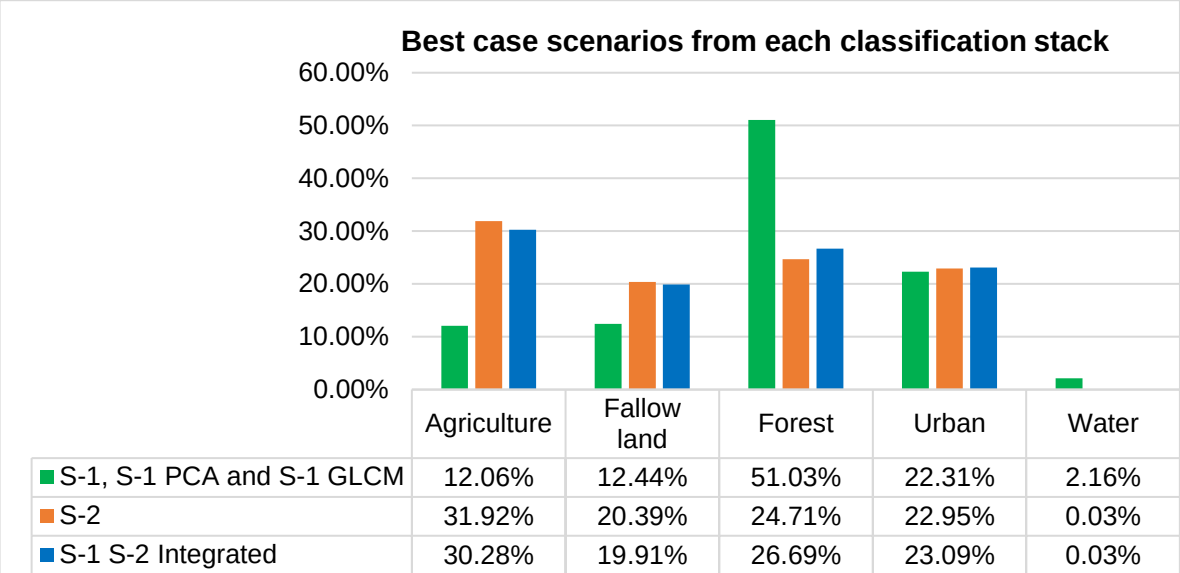

	Agriculture	Fallow land	Forest	Urban	Water
S-1, S-1 PCA and S-1 GLCM	12.06%	12.44%	51.03%	22.31%	2.16%
S-2	31.92%	20.39%	24.71%	22.95%	0.03%
S-1 S-2 Integrated	30.28%	19.91%	26.69%	23.09%	0.03%

Figure 3. 4: Best classification scenarios from Sentinel-1, Sentinel-2 and their integration

The data shown in Figure 3. 3 and Figure 3. 4 depicts that urban class classification is not considerably impacted across all image stacks (S-1, S-2, and their integration). However, there are noticeable distinctions between the classification of the forest and agriculture classes. In S-1, forest classes frequently invade other classes and misclassify their pixel values, having an impact on agriculture and fallow land. In addition, shadow pixels in S-1 with low backscattering values, which are classified as water in uneven and steep terrain, have increased the water class's coverage.

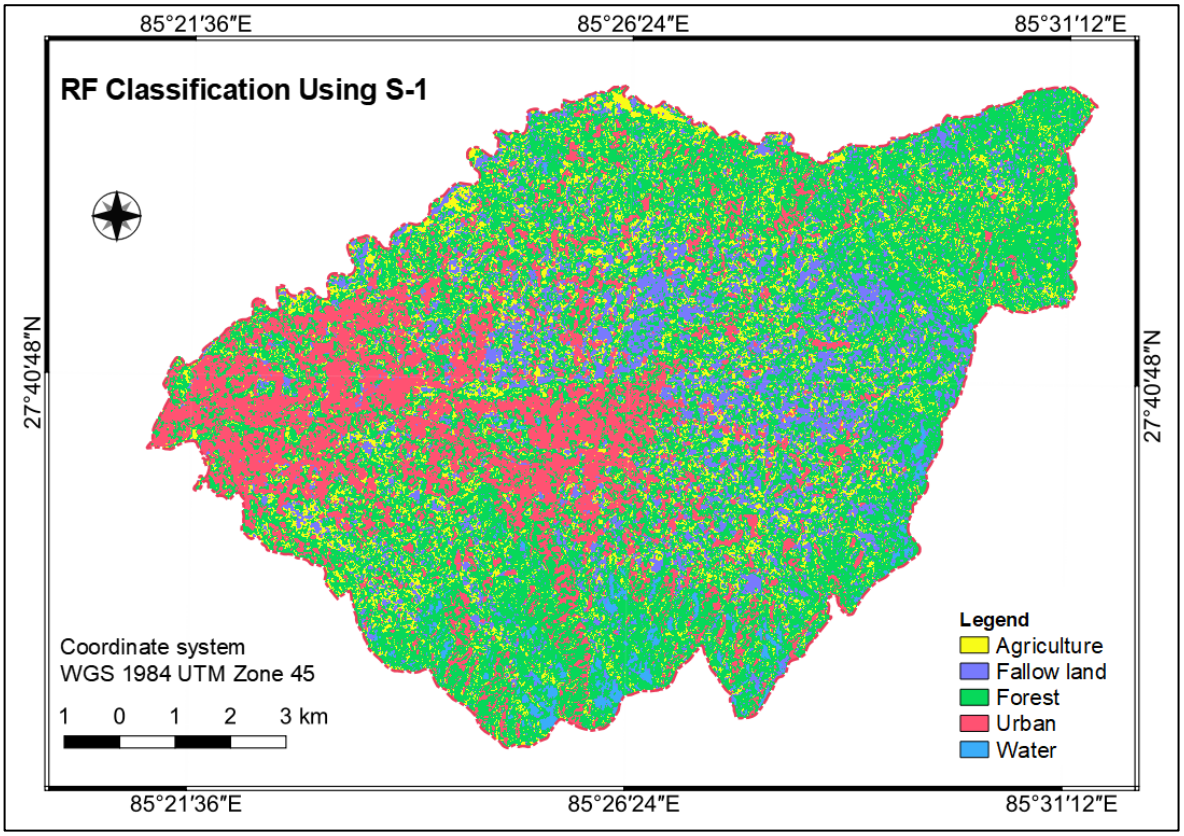

Map 3.4: Random Forest classification using Sentinel-1image

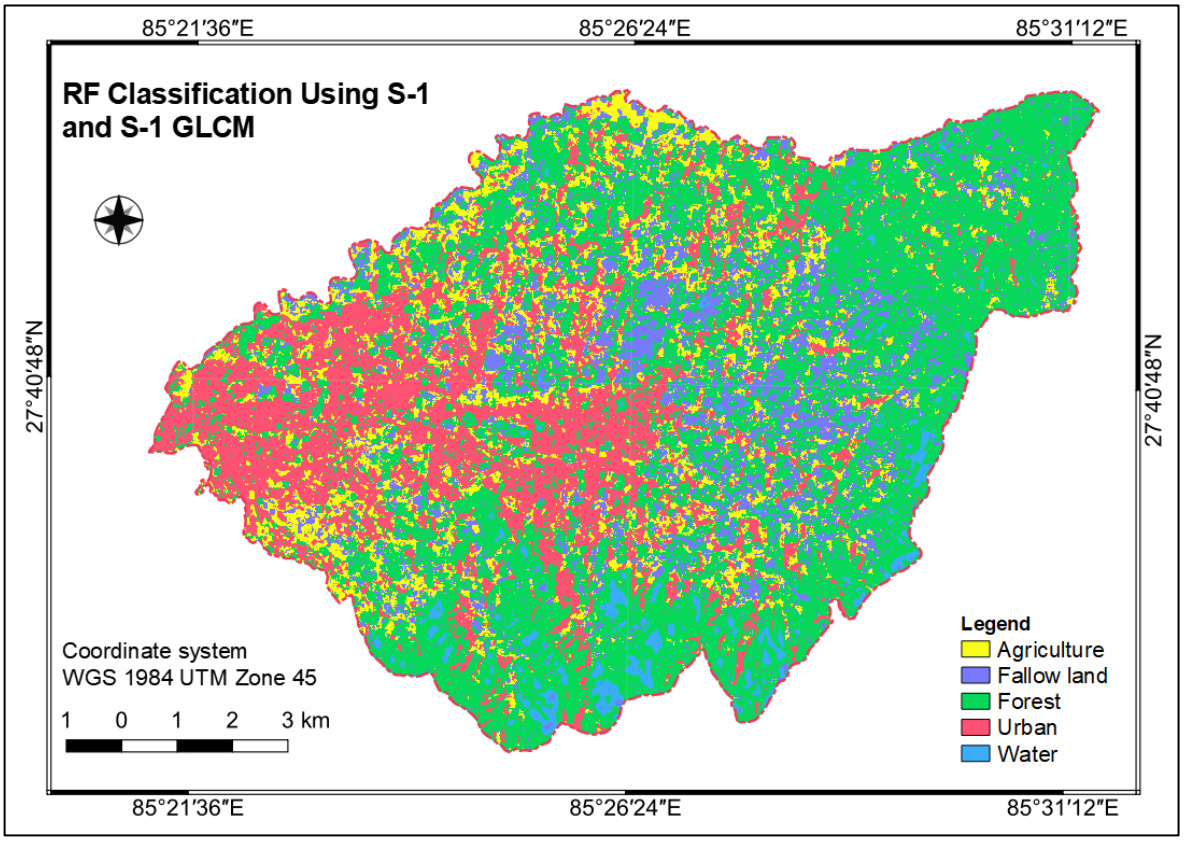

Map 3.5: Random Forest classification using Sentinel-1 and Sentinel-1 grey level cooccurrence matrix images

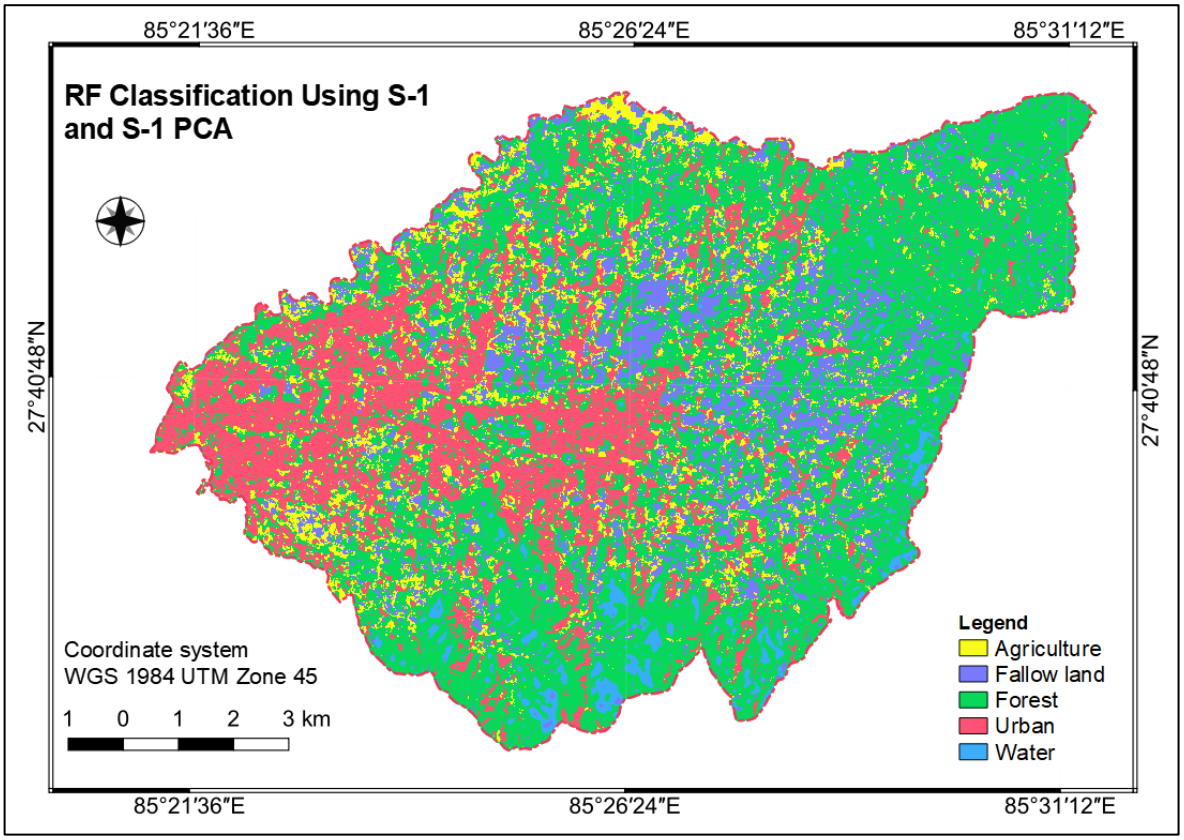

Map 3.6: Random Forest classification using Sentinel-1 and Sentinel-1 principal component analysis images

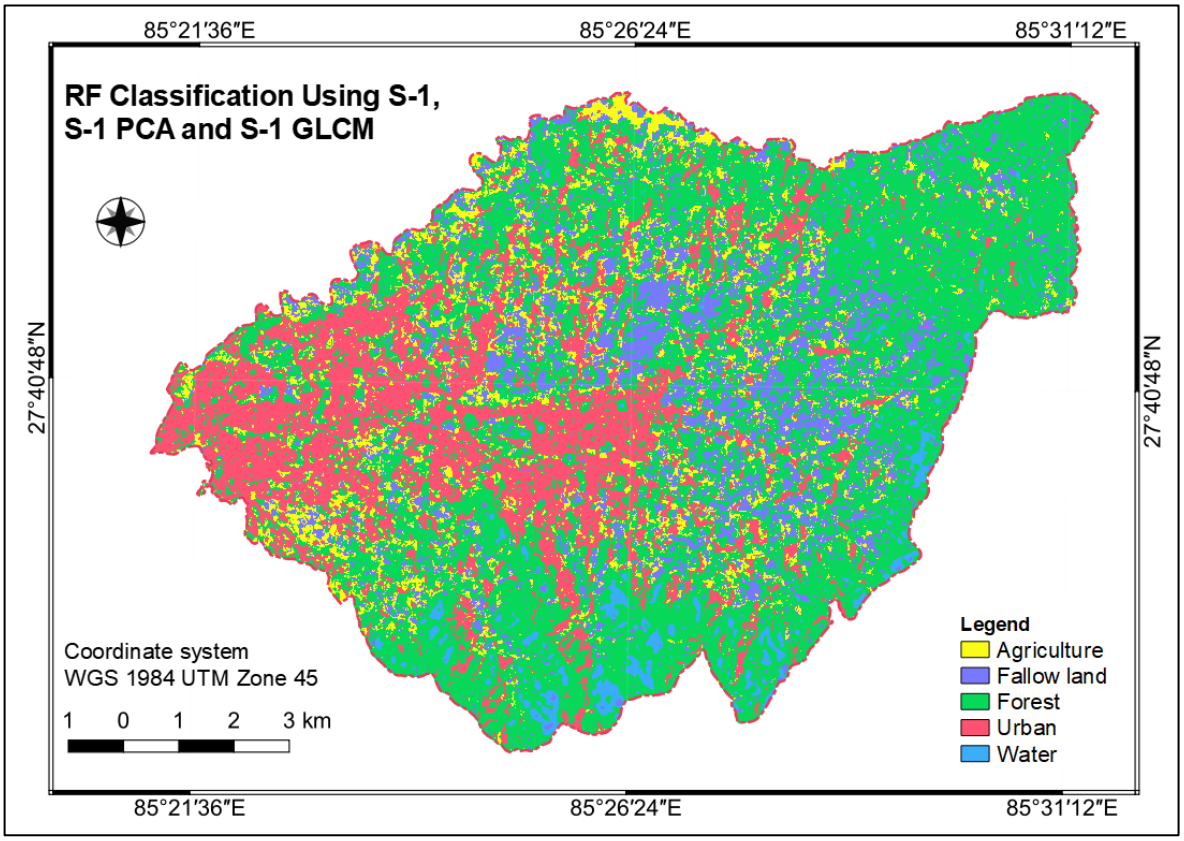

Map 3.7: Random Forest classification using Sentinel-1, Sentinel-1 principal component analysis and Sentinel-1 grey level cooccurrence matrix images

The creation of numerous maps and the corresponding data allowed for an evaluation of the employment of S-1 in conjunction with PCA and GLCM for LULC classification. The maps (Map 3.4, Map 3.5, Map 3.6 and Map 3.7) and Table 3. 1 in particular show how well various LULC classifications, including the forest class, may be classified. The findings show that the forest class has been significantly misclassified as various LULC classes, including water and urban regions. Particularly, the actual forest pixels with shadows were incorrectly classified as water pixels, highlighting a drawback in the classification method. Since proper classification of forested areas is crucial, the maps and statistics created may not be trustworthy sources of information for subsequent use. S-1 with PCA and GLCM, which was the best method in the comparison among the S-1 stacks generated the best results.

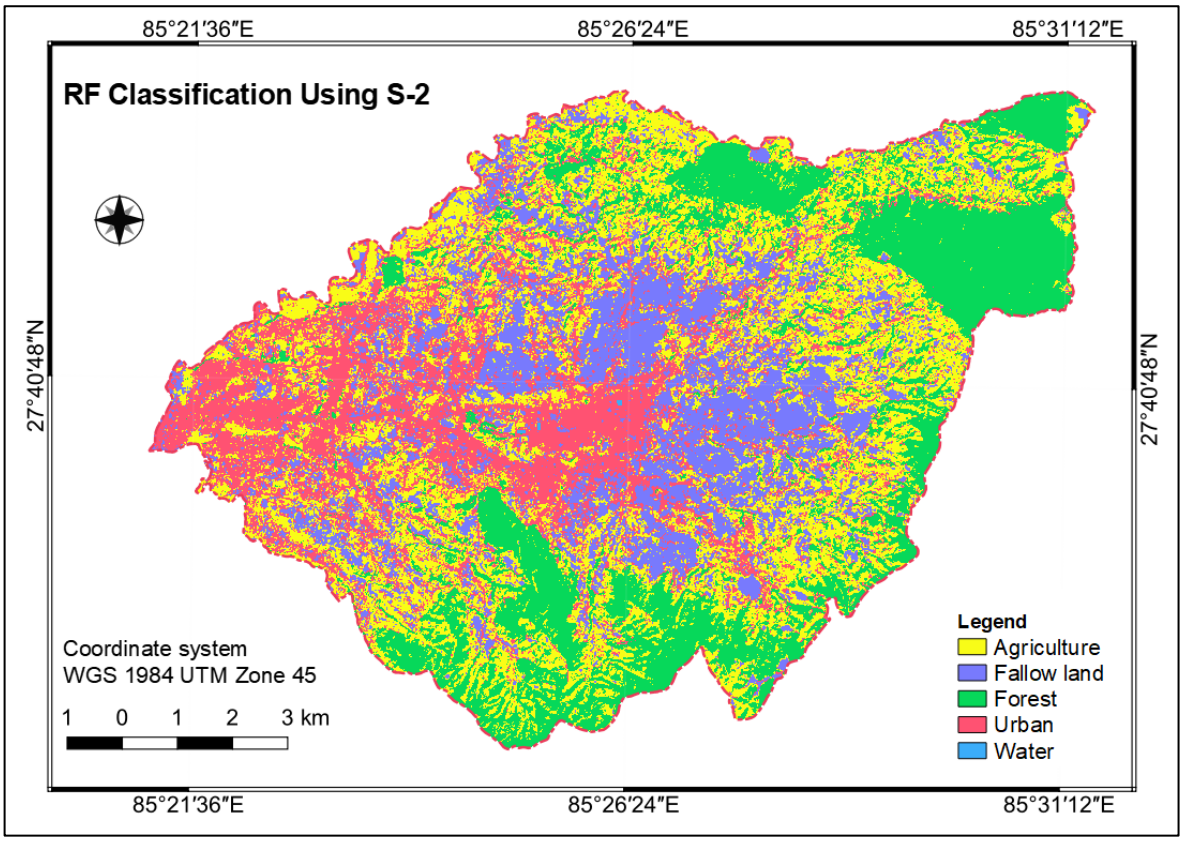

Map 3.8: Random Forest classification using Sentinel-2 image

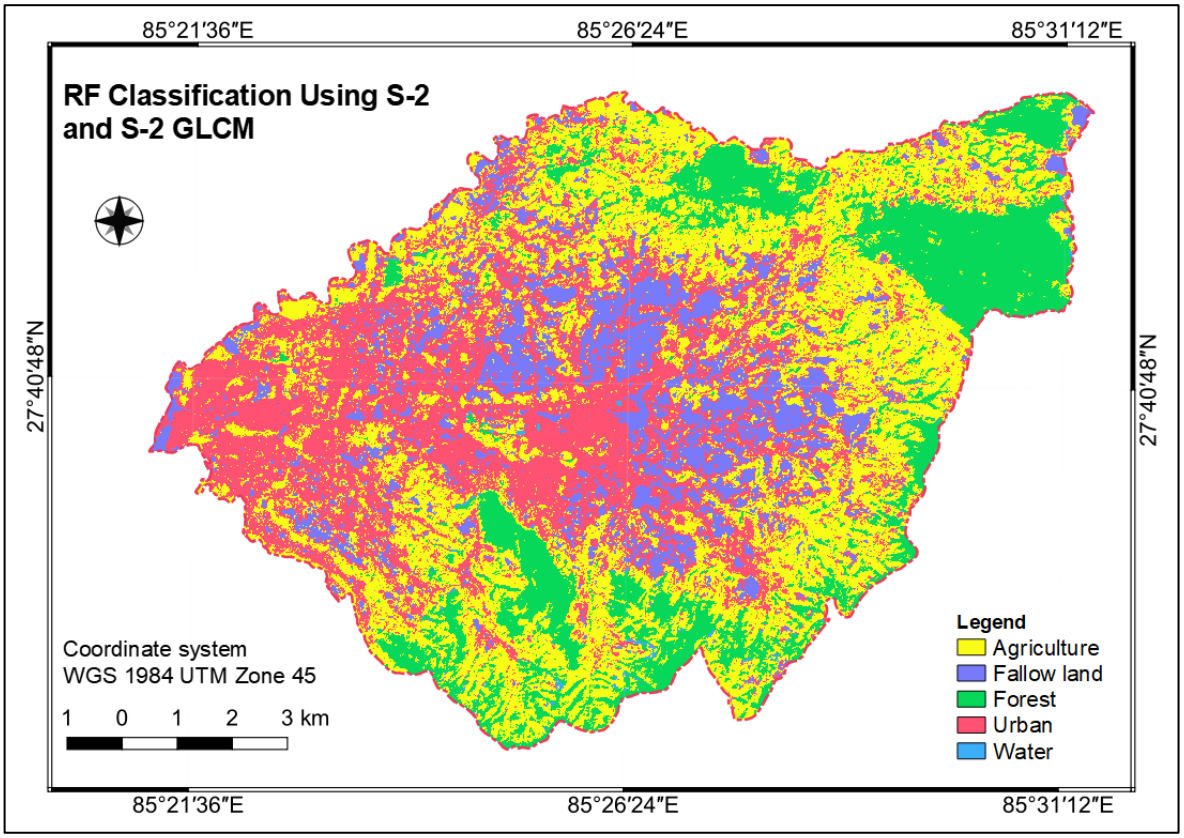

Map 3.9: Random Forest classification using Sentinel-2 and Sentinel-2 grey level cooccurrence matrix images

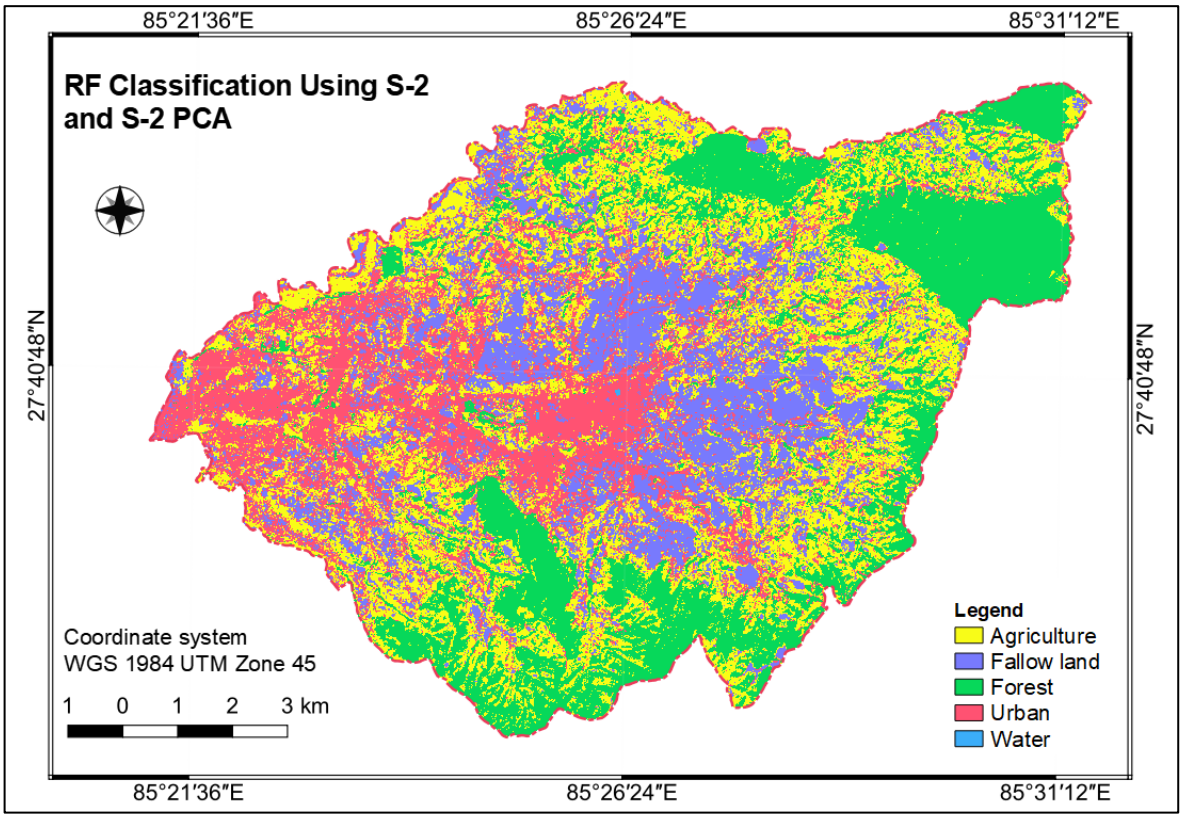

Map 3.10: Random Forest classification using Sentinel-2 and Sentinel-2 principal component analysis images

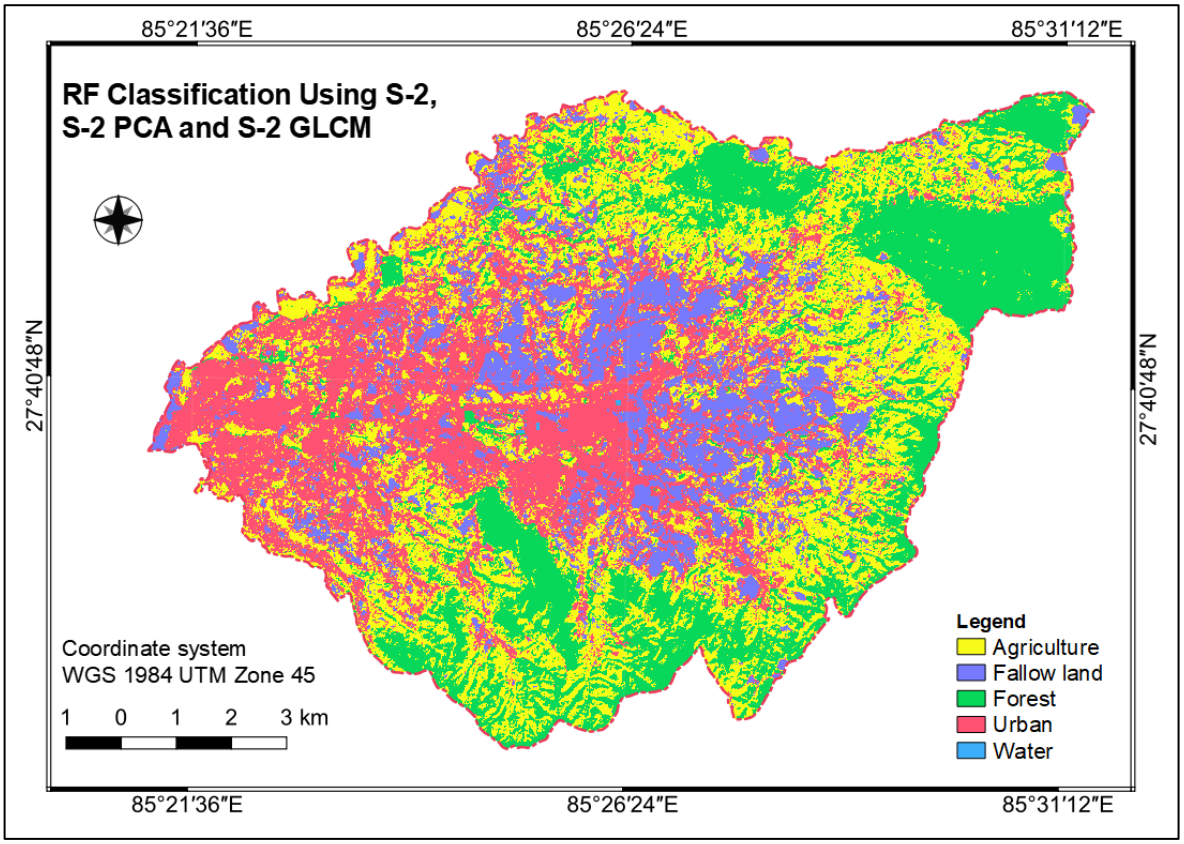

Map 3.11: Random Forest classification using Sentinel-2, Sentinel-2 principal component analysis and Sentinel-2 grey level cooccurrence matrix images

Significant variations were found between the LULC classification outcomes obtained with S-1 with PCA and GLCM and those obtained with S-2 with PCA. With an increase of almost 14%, the maps Map 3.8, Map 3.9, Map 3.10, and Map 3.11 in particular show that the overall classification accuracy was higher with S-2 data than with S-1, PCA, and GLCM. The best classification outcomes, however, were from S-2 data alone when compared to other S-2 data combinations with PCA and GLCM. However accurate the classification of some LULC classes was with S-2 data, there were significant limitations. For instance, the forest class was frequently misclassified as water when S-2 data and GLCM were merged, highlighting a drawback in this method. However, when S-2 data and PCA were combined, the classification results were more accurate and dependable, especially when smaller pixels that had fewer relationships with other classes were being classified.

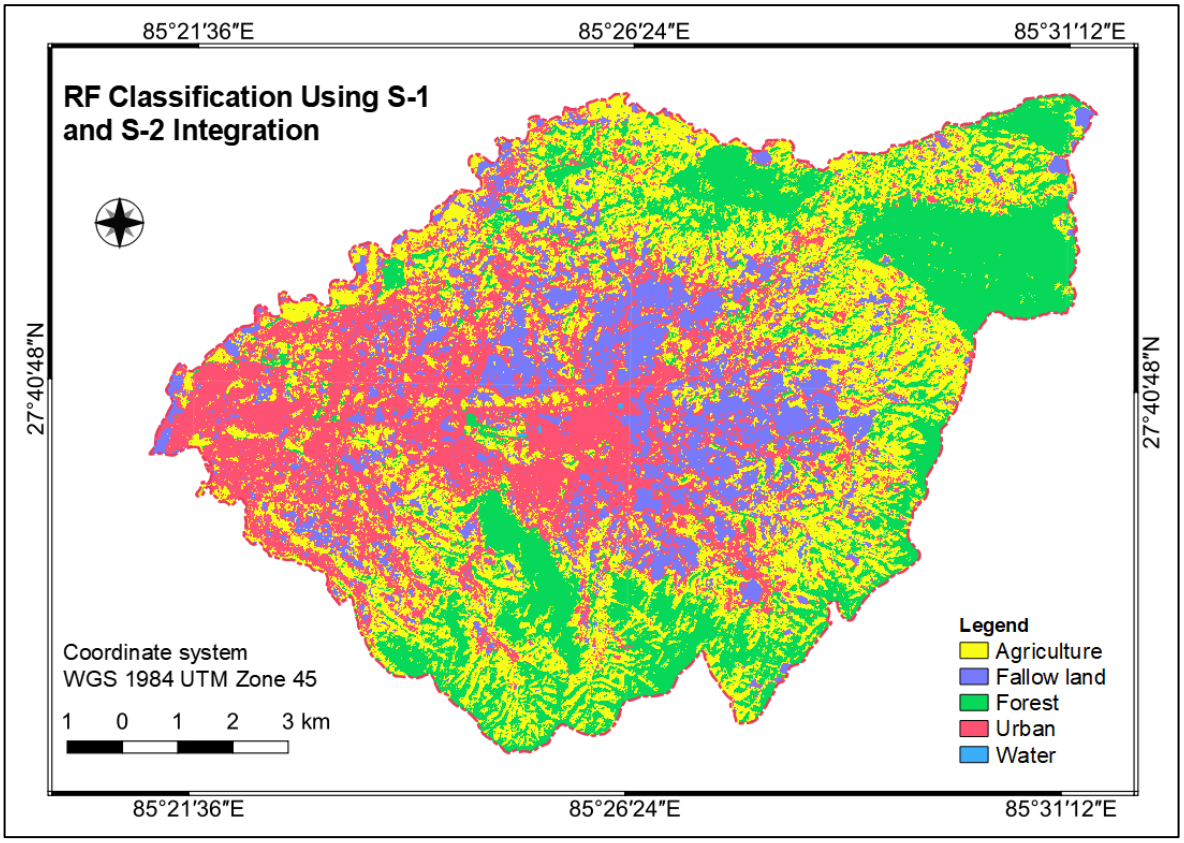

Map 3.12: Random Forest classification using Sentinel-1 Sentinel-2 integrated image

After comparing the various classification approaches, it was found that the integrated image delivered the best outcomes. This method gets beyond the previously noted drawbacks of employing S-1, S-2, and its PCA and GLCM combinations. The integrated image improved LULC class differences, particularly in differentiating fallow land from urban areas, fallow land from agriculture, etc. Despite the integrated image approach's increased accuracy, some misclassifications continue to occur, especially when it comes to vegetation and water features. For instance, rivers are incorrectly categorized as urban areas whereas grasses close to a forest are classed as agriculture. Refer Map 3.12 for detailed visual interpretation.

3.3. Comparison of Classification Accuracy

The S-1 and S-2 integrated image produced the best classification, with an OA of 91.06 percent and a Cohen's Kappa of 0.88. S-1 and its PCA have the lowest OA, at 54.05 percent, and the lowest Cohen's Kappa is 0.36. (Table 3. 2). Both in the best-case and worst-case classification stacks, the producer and user accuracies are similarly impacted.

Table 3. 2: Overall accuracy and Cohen's Kappa for each image stack ranked in order or accuracy

Original image	Processed image	Overall accuracy	Overall accuracy rank	Cohen's Kappa	Cohen's Kappa rank
Sentinel-1		57.52%	8	0.43	8
Sentinel-1	GLCM	63.77%	7	0.50	7
Sentinel-1	PCA	54.05%	9	0.36	9
Sentinel-1	GLCM, PCA	69.59%	6	0.57	6
Sentinel-2		83.07%	2	0.77	2
Sentinel-2	GLCM	81.89%	4	0.75	3
Sentinel-2	PCA	82.06%	3	0.75	4
Sentinel-2	GLCM, PCA	80.46%	5	0.73	5
Sentinel-1 & Sentinel-2	Integrated	91.06%	1	0.88	1

Table 3. 3: Error matrix of Sentinel-1 image with classification results

	S-1 Validation						
Class	**Agriculture**	**Fallow land**	**Forest**	**Urban**	**Water**	**Total**	**User accuracy**
Agriculture	32	5	15	3	0	55	**58.18%**
Fallow land	0	12	5	1	0	18	**66.67%**
Forest	7	2	14	3	0	26	**53.85%**
Urban	4	3	10	30	0	47	**63.83%**
Water	0	0	3	0	1	4	**25.00%**
Total	43	22	47	37	1	150	
Producer accuracy	**74.42%**	**54.55%**	**29.79%**	**81.08%**	**100.00%**		
Overall accuracy		**57.27 %**					
Cohen's Kappa		**0.43**					

Table 3. 4: Error matrix for the Sentinel-1 and Sentinel-1 grey level cooccurrence matrix images with classification results

	S-1 and S-1 GLCM Validation						
Class	**Agriculture**	**Fallow land**	**Forest**	**Urban**	**Water**	**Total**	**User accuracy**
Agriculture	38	5	7	5	0	55	**69.09%**
Fallow land	3	11	3	1	0	18	**61.11%**
Forest	8	3	15	0	0	26	**57.69%**
Urban	5	2	3	37	0	47	**78.72%**
Water	1	0	2	0	1	4	**25.00%**
Total	55	21	30	43	1	150	
Producer accuracy	**69.09%**	**52.38%**	**50.00%**	**86.05%**	**100.00%**		
Overall accuracy		**63.77%**					
Cohen's Kappa		**0.50**					

Table 3. 5: Error matrix for the Sentinel-1 and Sentinel-1 principal component analysis images with classification results

	S-1 and S-1 PCA Validation						
	Agriculture	**Fallow land**	**Forest**	**Urban**	**Water**	**Total**	**User accuracy**
Agriculture	37	6	5	7	0	55	**67.27%**
Fallow land	3	12	3	0	0	18	**66.67%**
Forest	9	3	11	3	0	26	**42.31%**
Urban	8	0	5	33	0	46	**71.74%**
Water	1	0	3	0	1	5	**20.00%**
Total	58	21	27	43	1	150	
Producer accuracy	**63.79%**	**57.14%**	**40.74%**	**76.74%**	**100.00%**		
Overall accuracy		**54.05%**					
Cohen's Kappa		**0.36**					

Table 3. 6: Error matrix for the Sentinel-1, Sentinel-1 principal component analysis and Sentinel-1 grey level cooccurrence matrix images with classification results

	S-1, S-1 PCA and S-1 GLCM Validation						
	Agriculture	**Fallow land**	**Forest**	**Urban**	**Water**	**Total**	**User accuracy**
Agriculture	48	2	1	4	0	55	**87.27%**
Fallow land	5	12	1	0	0	18	**66.67%**
Forest	5	2	17	2	0	26	**65.38%**
Urban	8	0	3	35	0	46	**76.09%**
Water	0	0	4	0	1	5	**20.00%**
Total	66	16	26	41	1	150	
Producer accuracy	**72.73%**	**75.00%**	**65.38%**	**85.37%**	**100.00%**		
Overall accuracy		**69.59%**					
Cohen's Kappa		**0.57**					

The accuracy results obtained by employing S-1 alone and in conjunction with GLCM and PCA are presented in the Table 3. 3, Table 3. 4,

Table 3. 5 and

Table 3. 6 . The results show that the OA and Cohen's Kappa have improved when the original image was used with PCA and GLCM. Although the water class has the lowest user accuracy, it has the highest producer accuracy. Forest regions are difficult for the classifier to recognize, although it does well with all water classifications. Additionally, the urban class has the highest accuracy rate while just one-fourth of water pixels are accurately identified by the classifier.

Table 3. 7: Error matrix for the Sentinel-2 image with classification results

	S-2 Validation						
	Agriculture	**Fallow land**	**Forest**	**Urban**	**Water**	**Total**	**User accuracy**
Agriculture	42	5	6	2	0	55	**76.36%**
Fallow land	0	17	0	1	0	18	**94.44%**
Forest	1	0	24	1	0	26	**92.31%**
Urban	7	5	1	34	0	47	**72.34%**
Water	0	0	0	0	4	4	**100.00%**
Total	50	27	31	38	4	150	
Producer accuracy	**84.00%**	**62.96%**	**77.42%**	**89.47%**	**100.00%**		
Overall accuracy		**83.07%**					
Cohen's Kappa		**0.77**					

Table 3. 8: Error matrix for the Sentinel-2 and Sentinel-2 grey level cooccurrence matrix images with classification results

	S-2 and S-2 GLCM Validation						
	Agriculture	**Fallow land**	**Forest**	**Urban**	**Water**	**Total**	**User accuracy**
Agriculture	46	1	8	0	0	55	**83.64%**
Fallow land	1	15	0	2	0	18	**83.33%**
Forest	1	0	25	0	0	26	**96.15%**
Urban	10	2	1	34	0	47	**72.34%**
Water	0	0	3	0	1	4	**25.00%**
Total	58	18	37	36	1	150	
Producer accuracy	**79.31%**	**83.33%**	**67.57%**	**94.44%**	**100.00%**		
Overall accuracy		**81.89%**					
Cohen's Kappa		**0.75**					

Table 3. 9: Error matrix for the Sentinel-2 and Sentinel-2 principal component analysis images with classification results

	S-2 and S-2 PCA Validation						
	Agriculture	**Fallow land**	**Forest**	**Urban**	**Water**	**Total**	**User accuracy**
Agriculture	48	4	3	0	0	55	**87.27%**
Fallow land	1	13	0	4	0	18	**72.22%**
Forest	2	0	24	0	0	26	**92.31%**
Urban	9	3	1	34	0	47	**72.34%**
Water	0	0	0	0	4	4	**100.00%**
Total	60	20	28	38	4	150	
Producer accuracy	**80.00%**	**65.00%**	**85.71%**	**89.47%**	**100.00%**		
Overall accuracy		**82.06%**					
Cohen's Kappa		**0.75**					

Table 3. 10: Error matrix for the Sentinel-2, Sentinel-2 principal component analysis and Sentinel-2 grey level cooccurrence matrix images with classification results

	S-2, S-2 PCA and S-2 GLCM Validation						
	Agriculture	**Fallow land**	**Forest**	**Urban**	**Water**	**Total**	**User accuracy**
Agriculture	49	2	4	0	0	55	**89.09%**
Fallow land	0	16	0	2	0	18	**88.89%**
Forest	2	0	23	1	0	26	**88.46%**
Urban	10	7	2	28	0	47	**59.57%**
Water	0	0	0	0	4	4	**100.00%**
Total	61	25	29	31	4	150	
Producer accuracy	**80.33%**	**64.00%**	**79.31%**	**90.32%**	**100.00%**		
Overall accuracy		**80.46%**					
Cohen's Kappa		**0.73**					

The

Table 3. 7,

Table 3. 8, Table 3. 9 and Table 3. 10 reflect the accuracy results obtained when S-2 was used both independently and in conjunction with GLCM and PCA. The results indicate that the OA and Cohen's Kappa have decreased as a result of applying PCA and GLCM on the original image. The accuracy of both users and producers has likewise decreased. For instance, the user accuracy of water has decreased by 25 percent as a result of the employment of GLCM. Despite an improvement in producer accuracy for fallow land and agriculture, the Cohen's Kappa and OA have declined.

Table 3. 11: Error matrix for the Sentinel-1 and Sentinel-2 integrated image with classification results

	S-1 S-2 integrated Validation						
	Agriculture	**Fallow land**	**Forest**	**Urban**	**Water**	**Total**	**User accuracy**
Agriculture	48	0	6	1	0	55	**87.27%**
Fallow land	1	17	0	0	0	18	**94.44%**
Forest	1	0	25	0	0	26	**96.15%**
Urban	3	2	1	41	0	47	**87.23%**
Water	0	0	1	0	3	4	**75.00%**
Total	53	19	33	42	3	150	
Producer accuracy	**90.57%**	**89.47%**	**75.76%**	**97.62%**	**100.00%**		
Overall accuracy		**91.06 %**					
Cohen's Kappa		**0.88**					

There has generally been an improvement in user and producer accuracy for all classes as compared to the S-1, S-2, and PCA/GLCM combination of the previous. The OA as well as the Cohen's Kappa have increased as a result. However, there is a problem with the forest class since, as indicated in Table 3. 11, it is not properly classified because of its similarity to agriculture. Despite this problem, user accuracy indicates that all other classes' reliability is generally satisfactory. The only exception is the water class, which has fewer samples

than other classes because of its low fraction of the classification image's coverage. Details are provided in Table 3. 11.

3.4. Discussions

3.4.1. Use of Principal Component Analysis and Grey Level Cooccurrence Matrix

The principal component analysis (PCA) and grey level cooccurrence matrix (GLCM) worked for the S-1 image increasing the accuracy about 12 percent and it did not work well for the S-2 images and its combination. There are some possible reasons.

First, PCA reduces the size of the image, but at the expense of losing crucial data necessary for precise classification. Additionally, it might not be a major indicator of improving accuracy (Janecek et al., 2008). However, GLCM increased the dimensionality of the data and added noise because it performs better with noisy images than with noiseless images (Beliakov et al., 2008). Additionally, the results demonstrated a reduction in accuracy when using S-2 image and an increase when using S-1 image.

Second, it is crucial to choose the most relevant characteristics for the classification operation in addition to minimizing the dimensionality of the data. RF classification uses a portion of randomly chosen features at each split, which makes it less sensitive to irrelevant or redundant features. However, the computational cost of the technique may grow and its accuracy may decrease if there are too many features included.

Third, when the dataset is too little or the model is too complicated, RF classification is susceptible to overfitting or underfitting. The addition of extra features (such PCA components or GLCM features) may make the model more complex and subject to overfitting.

3.4.2. Significance of Distribution of Land Use and Land Cover Classes

Land use and land cover are essential in advancing environmental management, sustainable development, and efficient decision-making. LULC has historically been created by the federal government in the Nepalese district of Bhaktapur but has not been successfully implemented. However, there has recently been a surge of effort to submit LULC data to the local level for validation in order to facilitate more effective policy-making

and planning. A recent study contributes to these efforts by offering knowledge that may be applied to enhance municipal planning and decision-making procedures.

The study emphasizes the importance of the study by showcasing findings that demonstrate the wide range of LULC in the Bhaktapur district. According to the integrated image analysis, the urban area only makes up around 23 percent of the total area, meaning that there is still a sizable amount of land that may be used for effective settlement design and urban center administration. However, there is a significant amount of barren land (19.91%), which brick factories are using and contaminating the urban environment. There is a need to either manage the settlement or transfer the brick factories because the urban and industrial areas overlap in eastern part of Bhaktapur.

A majority of the land (30.28 percent) is still used for agriculture, which is practiced year-round utilizing both conventional farming methods and tunnel farming. Ponds (0.03 percent) and other bodies of water have been accurately mapped in the area, but rivers flowing into and through the boundaries have not because of their high turbidity. This creates a problem for river trash management that requires considerable attention. The region's ecosystem and temperature are significantly maintained and controlled by the forest area, which accounts for 26.69 percent of the total land area. Although the forests are well-kept, there are still bushy patches with small tress alongside the settlement in the hills that help to keep the soil stable.

These findings differ somewhat from those of previous research conducted in the Bhaktapur district, for example (Thapa Chhetri & Moriwaki, 2017) has estimated that forests (30.1%), agriculture/shrubs (36.7%), and urban (9.0 percent). It might be because the author used Landsat images, the period of acquisition was in September 2015, which is not yet dry season, and the definition of class is slightly different; for example, shrubs are included in agricultural, while the current research has accommodated them in the forest class.

3.4.3. Integration Sentinel-1 and Sentinel-2 for Land Use and Land Cover Mapping

The study of integrating S-1 and S-2 for LULC classification using RF classification looked at a number of benefits. One of the main benefits of using data from both sensors is improved classification accuracy when compared to using individual images. Improved feature selection and better identification of complex landscapes, such as areas with a mix of terrain types or classes are to account for this. By integrating the data from the two sensors, a more thorough picture of the area could be created, enabling the creation of training samples and a more precise LULC classification. S-1 and S-2 have temporal resolutions that are limited to one week, after which significant biological or physical change won't occur. It makes things easier.

3.5. Limitations of the Study

Due to the presence of aquatic plants and other micro-biotic species, the spectral signatures of the water in the ponds with less water is closer with those of vegetation; as a result, they are not classified. The water percentage, however, may have gone up by 0.5 percent as a result of the spatial resolution of S-2 and the GLCM measures applied to S-1.

To increase the accuracy of the classification, more data combinations could be used, such as the use of spectral indices. Ceccato et al. (2002) developed a method that improved classification accuracy for determining the water content of vegetation using a spectral index from remotely sensed data. The classification accuracy is often increased by 4 to 5 percent when S-1 VH polarization measurements are integrated with S-2 data, compared to when using only optical data (Khan et al., 2020).

The S-1 images of two time periods that represents the two seasons are coregister for improved classification but was left for the S-2 images. There may have been both positive or negative effects which requires thorough investigation. For example, it has the potential to increase accuracy through improved feature representation and discrimination, but it can also create difficulties due to seasonal variation and increasing data complexity.

It was challenging to carry out the research as thoroughly as was expected due to time constraints and the advancement of the current methodology in different aspect.

4. Chapter- 4: Conclusions and Recommendations

For land use and land cover classification mapping employing RF classification in five different classes (agriculture, fallow land, forest, urban, and water), the study set out to evaluate the LULC accuracy of integrated, optical, and SAR datasets as well as texture and dimension reduction methods. The study also made an effort to demonstrate the effectiveness of S-1 and S-2 images for LULC mapping in the study region. S-1 and S-2 integration produced the best results, but the S-2 image with PCA performed the lowest. The complementary nature of the images explains why the integrated image outperformed the S-2 PCA performance, which was probably poor as a result of the increased dimensionality that arose from stacking the associated bands together during classification, which confused the classifier. S-1, which only has two polarizations and has a poor classification performance, exhibited an improvement. The inclusion of GLCM and PCA components helped to increase the classification's accuracy to some extent.

With an effort to create LULC classification maps, S-1 and S-2 have been combined for the first time in the study area, and the results' adequate accuracy enable local-level evidence-based planning and decision-making. In future investigations using convolutional neural network (CNN) and artificial neural network (ANN) models, the researchers could use additional fusion methodologies to add milestones to the current research domain. Additionally, integrating a variety of imagery, such as radar, multispectral satellite, and high-resolution unmanned aerial vehicle (UAV) images, may result in more accurate results than what we now have. The researchers must, however, take care to prevent overfitting the classifier or to just match the classifier to the needs and possibilities of the model. Regarding the use of PCA and GLCM, the use of principal components and the each GLCM measures if tested different could amplify the classification accuracy even with S-2 image.

Along with using several strategies, the technique's spectral indices might enhance classification accuracy. Indexes like the Normalized Difference Vegetation Index (NDVI) and the Enhanced Vegetation Index (EVI) are often used to assess vegetation cover, health, and biomass. By merging various bands, these indices can decrease the effects of atmospheric disturbances, sensor noise, and illumination changes, improving classification accuracy. Spectral indices can also be used to differentiate between different LULC classes by comparing their spectral signatures. In general, using spectral indices can be a helpful method to improve LULC mapping accuracy, especially in the Bhaktapur district.

References

Abdi, H., & Williams, L. J. (2010). Principal component analysis: Principal component analysis. *Wiley Interdisciplinary Reviews: Computational Statistics*, *2*(4), 433–459. https://doi.org/10.1002/wics.101

Acharya, K., & Dangi, R. (2010, January). *Case Studies on Measuring and Assessing Forest Degradation in Nepal: Review of Data and Methods*. Forest Resources Assessment Working Paper 163, FAO, Italy. https://www.researchgate.net/publication/272354185_Case_Studies_on_Measuring_and_Assessing_Forest_Degradation_in_Nepal_Review_of_Data_and_Methods

Aggarwal, S. (2004). Principles of remote sensing. *Satellite Remote Sensing and GIS Applications in Agricultural Meteorology*, *23*(2), 23–28.

Alfrey, G. F. (1981). Remote Sensing: Optics and Optical Systems. *Physics Bulletin*, *32*(3), 83–83. https://doi.org/10.1088/0031-9112/32/3/048

Anderson, J. R. (1971). Land-use classification schemes. *Photogrammetric Engineering*.

Anderson, J. R. (1976). *A land use and land cover classification system for use with remote sensor data* (Vol. 964). US Government Printing Office.

Bae, J., & Ryu, Y. (2015). Land use and land cover changes explain spatial and temporal variations of the soil organic carbon stocks in a constructed urban park. *Landscape and Urban Planning*, *136*, 57–67.

Balzter, H., Cole, B., Thiel, C., & Schmullius, C. (2015). Mapping CORINE Land Cover from Sentinel-1A SAR and SRTM Digital Elevation Model Data using Random Forests. *Remote Sensing*, *7*(11), 14876–14898. https://doi.org/10.3390/rs71114876

Beliakov, G., James, S., & Troiano, L. (2008). Texture recognition by using GLCM and various aggregation functions. *2008 IEEE International Conference on Fuzzy Systems (IEEE World Congress on Computational Intelligence)*, 1472–1476. https://doi.org/10.1109/FUZZY.2008.4630566

Campbell, J. B., & Wynne, R. H. (2011). *Introduction to remote sensing*. Guilford Press.

Canada, K. E. S., & Department of Topography, N., Government of Nepal, Kathmandu. (1986). Land Resource Mapping Project. *Land Utilization Report*, *112*.

Chachondhia, P., Shakya, A., & Kumar, G. (2021). Performance evaluation of machine learning algorithms using optical and microwave data for LULC classification. *Remote Sensing Applications: Society and Environment*, *23*, 100599. https://doi.org/10.1016/j.rsase.2021.100599

Chang, Y., Hou, K., Li, X., Zhang, Y., & Chen, P. (2018). Review of Land Use and Land Cover Change research progress. *IOP Conference Series: Earth and Environmental Science*, *113*, 012087. https://doi.org/10.1088/1755-1315/113/1/012087

Chatziantoniou, A., Psomiadis, E., & Petropoulos, G. (2017). Co-Orbital Sentinel 1 and 2 for LULC Mapping with Emphasis on Wetlands in a Mediterranean Setting Based on Machine Learning. *Remote Sensing*, *9*(12), 1259. https://doi.org/10.3390/rs9121259

Chen, Q., Chen, H., Zhang, J., Hou, Y., Shen, M., Chen, J., & Xu, C. (2020). Impacts of climate change and LULC change on runoff in the Jinsha River Basin. *Journal of Geographical Sciences*, *30*, 85–102.

Choi, B. G., Na, Y. W., Kim, S. H., & Lee, J. I. (2014). A Study on the Improvement classification accuracy of Land Cover using the Aerial hyperspectral image with PCA. *Journal of Korean Society for Geospatial Information System*, *22*(1), 81–88. https://doi.org/10.7319/kogsis.2014.22.1.081

Cihlar, J. (2000). Land cover mapping of large areas from satellites: Status and research priorities. *International Journal of Remote Sensing*, *21*(6–7), 1093–1114.

Cihlar, J., & Jansen, L. J. M. (2001). From Land Cover to Land Use: A Methodology for Efficient Land Use Mapping over Large Areas. *The Professional Geographer*, *53*(2), 275–289. https://doi.org/10.1080/00330124.2001.9628460

Clerici, N., Valbuena Calderón, C. A., & Posada, J. M. (2017). Fusion of Sentinel-1A and Sentinel-2A data for land cover mapping: A case study in the lower Magdalena region, Colombia. *Journal of Maps*, *13*(2), 718–726. https://doi.org/10.1080/17445647.2017.1372316

Comber, A. J., Harris, P., & Tsutsumida, N. (2016). Improving land cover classification using input variables derived from a geographically weighted principal components analysis. *ISPRS Journal of Photogrammetry and Remote Sensing*, *119*, 347–360. https://doi.org/10.1016/j.isprsjprs.2016.06.014

Congalton, R. G. (1991). A review of assessing the accuracy of classifications of remotely sensed data. *Remote Sensing of Environment*, *37*(1), 35–46. https://doi.org/10.1016/0034-4257(91)90048-B

Dasari, K., Anjaneyulu, L., Jayasri, P. V., & Prasad, A. V. V. (2015). Importance of speckle filtering in image classification of SAR data. *2015 International Conference on Microwave, Optical and Communication Engineering (ICMOCE)*, 349–352. https://doi.org/10.1109/ICMOCE.2015.7489764

DDC Bhaktapur. (2023). *Brief Introduction: Bhaktapur Distrcit Development Committee*. Retrieved 10 April 2023, from https://dccbhaktapur.gov.np/en/brief-introduction/

Deng, J. S., Wang, K., Deng, Y. H., & Qi, G. J. (2008). PCA-based land-use change detection and analysis using multitemporal and multisensor satellite data. *International Journal of Remote Sensing*, *29*(16), 4823–4838. https://doi.org/10.1080/01431160801950162

Dong, J., Zhuang, D., Huang, Y., & Fu, J. (2009). Advances in Multi-Sensor Data Fusion: Algorithms and Applications. *Sensors*, *9*(10), 7771–7784. https://doi.org/10.3390/s91007771

Drusch, M., Del Bello, U., Carlier, S., Colin, O., Fernandez, V., Gascon, F., Hoersch, B., Isola, C., Laberinti, P., Martimort, P., Meygret, A., Spoto, F., Sy, O., Marchese, F., & Bargellini, P. (2012). Sentinel-2: ESA's Optical High-Resolution Mission for

GMES Operational Services. *Remote Sensing of Environment*, *120*, 25–36. https://doi.org/10.1016/j.rse.2011.11.026

FAO. (2023). *LAND COVER CLASSIFICATION SYSTEM*. Retrieved 16 April 2023, from https://www.fao.org/3/X0596E/x0596e01f.htm

Foody, G. M. (2002). Status of land cover classification accuracy assessment. *Remote Sensing of Environment*, *80*(1), 185–201. https://doi.org/10.1016/S0034-4257(01)00295-4

Gilmour, D. A., & Nurse, M. C. (1991). Farmer initiatives in increasing tree cover in central Nepal. *Mountain Research and Development*, 329–337.

Gislason, P. O., Benediktsson, J. A., & Sveinsson, J. R. (2004). Random forest classification of multisource remote sensing and geographic data. *IEEE International IEEE International IEEE International Geoscience and Remote Sensing Symposium, 2004. IGARSS '04. Proceedings. 2004*, *2*, 1049–1052. https://doi.org/10.1109/IGARSS.2004.1368591

Haack, B. N., & Rafter, A. (2006). Urban growth analysis and modeling in the Kathmandu Valley, Nepal. *Habitat International*, *30*(4), 1056–1065. https://doi.org/10.1016/j.habitatint.2005.12.001

Hale, S. R., & Rock, B. N. (2003). Impact of Topographic Normalization on Land-Cover Classification Accuracy. *Photogrammetric Engineering & Remote Sensing*, *69*(7), 785–791. https://doi.org/10.14358/PERS.69.7.785

Home: Corine Land Cover classes. (2023). Retrieved 16 April 2023, from https://land.copernicus.eu/user-corner/technical-library/corine-land-cover-nomenclature-guidelines/html

Janecek, A. G., & Gansterer, W. N. (2008). A comparison of classification accuracy achieved with wrappers, Filters and PCA. *Workshop on New Challenges for Feature Selection in Data Mining and Knowledge Discovery*.

Jensen, J. R. (1996). *Introductory digital image processing: A remote sensing perspective.* (Issue Ed. 2). Prentice-Hall Inc.

Jensen, J. R. (2009). *Remote sensing of the environment: An earth resource perspective 2/e*. Pearson Education India.

Jong-Sen Lee, Jen-Hung Wen, Ainsworth, T. L., Kun-Shan Chen, & Chen, A. J. (2009). Improved Sigma Filter for Speckle Filtering of SAR Imagery. *IEEE Transactions on Geoscience and Remote Sensing*, *47*(1), 202–213. https://doi.org/10.1109/TGRS.2008.2002881

Khan, A., Govil, H., Kumar, G., & Dave, R. (2020). Synergistic use of Sentinel-1 and Sentinel-2 for improved LULC mapping with special reference to bad land class: A case study for Yamuna River floodplain, India. *Spatial Information Research*, *28*(6), 669–681. https://doi.org/10.1007/s41324-020-00325-x

Khatami, R., Mountrakis, G., & Stehman, S. V. (2016). A meta-analysis of remote sensing research on supervised pixel-based land-cover image classification processes: General guidelines for practitioners and future research. *Remote Sensing of Environment*, *177*, 89–100. https://doi.org/10.1016/j.rse.2016.02.028

Kumar, R. S., Menaka, C., & Cutler, M. E. J. (2013). Ann Based Robust LULC Classification Technique Using Spectral, Texture and Elevation Data. *Journal of the Indian Society of Remote Sensing*, *41*(3), 477–486. https://doi.org/10.1007/s12524-012-0247-y

Kumar, S., & Singh, R. (2021). Geospatial Applications in Land Use/Land Cover Change Detection for Sustainable Regional Development: The Case of Central Haryana, India. *Geomatics and Environmental Engineering*, *15*(3), 81–98. https://doi.org/10.7494/geom.2021.15.3.81

Lanaras, C., Bioucas-Dias, J., Galliani, S., Baltsavias, E., & Schindler, K. (2018). Super-resolution of Sentinel-2 images: Learning a globally applicable deep neural network. *ISPRS Journal of Photogrammetry and Remote Sensing*, *146*, 305–319. https://doi.org/10.1016/j.isprsjprs.2018.09.018

Lee, J. S., Jurkevich, L., Dewaele, P., Wambacq, P., & Oosterlinck, A. (1994). Speckle filtering of synthetic aperture radar images: A review. *Remote Sensing Reviews*, *8*(4), 313–340. https://doi.org/10.1080/02757259409532206

Lillesand, T., Kiefer, R. W., & Chipman, J. (2015). *Remote sensing and image interpretation*. John Wiley & Sons.

Makar, R. S., & Shahin, S. A. (2022). Development of a PCA-based land use/land cover classification utilizing Sentinel-2time series. *Middle East Journal of Agriculture Research*. https://doi.org/10.36632/mejar/2022.11.2.42

Markham, B. L., & Townshend, J. R. (1981). *Land cover classification accuracy as a function of sensor spatial resolution*.

Natural Resources Canada. (2023). *Elements of Visual Interpretation*. Retrieved 12 April 2023, from https://natural-resources.canada.ca/maps-tools-and-publications/satellite-imagery-and-air-photos/tutorial-fundamentals-remote-sensing/image-interpretation-analysis/elements-visual-interpretation/9291

NSO, G. of N. (2023). *Population | National Population and and Housing Census 2021 Results*. Retrieved 9 April 2023, from https://censusnepal.cbs.gov.np/results/population?province=3&district=29

Nurfadila, J. S., Baja, S., Neswati, R., Rukmana, D., & Zylshal, Z. (2019). Initial Results on Landuse/Landcover Classification Using Pixel-Based Random Forest Algorithm on Sentinel-2 Imagery over Enrekang Region. *IOP Conference Series: Earth and Environmental Science*, *280*(1), 012036. https://doi.org/10.1088/1755-1315/280/1/012036

Olofsson, P., Foody, G. M., Herold, M., Stehman, S. V., Woodcock, C. E., & Wulder, M. A. (2014). Good practices for estimating area and assessing accuracy of land change. *Remote Sensing of Environment*, *148*, 42–57. https://doi.org/10.1016/j.rse.2014.02.015

Parsons, V. L. (2017). Stratified Sampling. In N. Balakrishnan, T. Colton, B. Everitt, W. Piegorsch, F. Ruggeri, & J. L. Teugels (Eds.), *Wiley StatsRef: Statistics Reference*

Online (1st ed., pp. 1–11). Wiley. https://doi.org/10.1002/9781118445112.stat05999.pub2

Paudel, B., Zhang, Y., Li, S., Liu, L., Wu, X., & Khanal, N. R. (2016). Review of studies on land use and land cover change in Nepal. *Journal of Mountain Science*, *13*(4), 643–660. https://doi.org/10.1007/s11629-015-3604-9

Pereira, L. de O., Freitas, C. da C., Sant´Anna, S. J. S., Lu, D., & Moran, E. F. (2013). Optical and radar data integration for land use and land cover mapping in the Brazilian Amazon. *GIScience & Remote Sensing*, *50*(3), 301–321. https://doi.org/10.1080/15481603.2013.805589

Rimal, B., Sharma, R., Kunwar, R., Keshtkar, H., Stork, N. E., Rijal, S., Rahman, S. A., & Baral, H. (2019). Effects of land use and land cover change on ecosystem services in the Koshi River Basin, Eastern Nepal. *Ecosystem Services*, *38*, 100963.

Salem, M., Tsurusaki, N., & Divigalpitiya, P. (2020). Land use/land cover change detection and urban sprawl in the peri-urban area of greater Cairo since the Egyptian revolution of 2011. *Journal of Land Use Science*, *15*(5), 592–606.

Schmidt, K., Schwerdt, M., Miranda, N., & Reimann, J. (2020). Radiometric Comparison within the Sentinel-1 SAR Constellation over a Wide Backscatter Range. *Remote Sensing*, *12*(5), 854. https://doi.org/10.3390/rs12050854

Sentinel 1: Satellite Imagery, Overview, And Characteristics. (2021, December 15). https://eos.com/find-satellite/sentinel-1/

Sentinel-1 Radiometric Calibration—ArcMap | Documentation. (2023). Retrieved 27 April 2023, from https://desktop.arcgis.com/en/arcmap/latest/manage-data/raster-and-images/sentinel-1-radiometric-calibration.htm

Sentinel-2—Overview—Sentinel Online—Sentinel Online. (2023). Retrieved 18 April 2023, from https://sentinel.esa.int/web/sentinel/missions/sentinel-2/overview

Silva, K. D. (2015). The spirit of place of Bhaktapur, Nepal. *International Journal of Heritage Studies*, *21*(8), 820–841. https://doi.org/10.1080/13527258.2015.1028962

Smith, J. H., Stehman, S. V., Wickham, J. D., & Yang, L. (2003). Effects of landscape characteristics on land-cover class accuracy. *Remote Sensing of Environment*, *84*(3), 342–349. https://doi.org/10.1016/S0034-4257(02)00126-8

Srivastava, A., Bharadwaj, S., Dubey, R., Sharma, V. B., & Biswas, S. (2022). MAPPING VEGETATION AND MEASURING THE PERFORMANCE OF MACHINE LEARNING ALGORITHM IN LULC CLASSIFICATION IN THE LARGE AREA USING SENTINEL-2 AND LANDSAT-8 DATASETS OF DEHRADUN AS A TEST CASE. *The International Archives of the Photogrammetry, Remote Sensing and Spatial Information Sciences*, *XLIII-B3-2022*, 529–535. https://doi.org/10.5194/isprs-archives-XLIII-B3-2022-529-2022

Staelin, D. H., & Kerekes, J. P. (1995). Combined microwave and optical atmospheric remote sensing techniques: A review. *Conference Proceedings Second Topical Symposium on Combined Optical-Microwave Earth and Atmosphere Sensing*, 3–6. https://doi.org/10.1109/COMEAS.1995.472358

Stehman, S. V. (2009). Sampling designs for accuracy assessment of land cover. *International Journal of Remote Sensing*, *30*(20), 5243–5272. https://doi.org/10.1080/01431160903131000

Sundaresan, A., Varshney, P. K., & Arora, M. K. (2007). Robustness of change detection algorithms in the presence of registration errors. *Photogrammetric Engineering & Remote Sensing*, *73*(4), 375–383.

Svoboda, J., Štych, P., Laštovička, J., Paluba, D., & Kobliuk, N. (2022). Random Forest Classification of Land Use, Land-Use Change and Forestry (LULUCF) Using Sentinel-2 Data—A Case Study of Czechia. *Remote Sensing*, *14*(5), 1189. https://doi.org/10.3390/rs14051189

Swift, C., Jones, W., & Grantham, W. (1980). Microwave remote sensing. *IEEE Antennas and Propagation Society Newsletter*, *22*(5), 4–9. https://doi.org/10.1109/MAP.1980.27489

Tassi, A., & Vizzari, M. (2020). Object-Oriented LULC Classification in Google Earth Engine Combining SNIC, GLCM, and Machine Learning Algorithms. *Remote Sensing*, *12*(22), 3776. https://doi.org/10.3390/rs12223776

Tavares, P., Beltrão, N., Guimarães, U., & Teodoro, A. (2019). Integration of Sentinel-1 and Sentinel-2 for Classification and LULC Mapping in the Urban Area of Belém, Eastern Brazilian Amazon. *Sensors*, *19*(5), 1140. https://doi.org/10.3390/s19051140

Thapa Chhetri, D. B., & Moriwaki, R. (2017). MONITORING URBAN GROWTH, LAND USE AND LAND COVER USING REMOTE SENSING AND GIS TECHNIQUES: A CASE STUDY OF BHAKTAPUR DISTRICT,NEPAL. *Engineering Science and Technology: An International Journal (ESTIJ)*, *7*, 32.

Uddin, K., Shrestha, H. L., Murthy, M. S. R., Bajracharya, B., Shrestha, B., Gilani, H., Pradhan, S., & Dangol, B. (2015). Development of 2010 national land cover database for the Nepal. *Journal of Environmental Management*, *148*, 82–90.

Valdivieso-Ros, C., Alonso-Sarria, F., & Gomariz-Castillo, F. (2023). Effect of the Synergetic Use of Sentinel-1, Sentinel-2, LiDAR and Derived Data in Land Cover Classification of a Semiarid Mediterranean Area Using Machine Learning Algorithms. *Remote Sensing*, *15*(2), 312. https://doi.org/10.3390/rs15020312

Virgo, K. J., & Subba, K. J. (1994). Land-use change between 1978 and 1990 in Dhankuta district, Koshi Hills, eastern Nepal. *Mountain Research and Development*, 159–170.

Vivekananda, G., Swathi, R., & Sujith, A. (2021). Multi-temporal image analysis for LULC classification and change detection. *European Journal of Remote Sensing*, *54*(sup2), 189–199. https://doi.org/10.1080/22797254.2020.1771215

Wang, S. W., Gebru, B. M., Lamchin, M., Kayastha, R. B., & Lee, W.-K. (2020). Land Use and Land Cover Change Detection and Prediction in the Kathmandu District of Nepal Using Remote Sensing and GIS. *Sustainability*, *12*(9), 3925. https://doi.org/10.3390/su12093925

Welcome to the QGIS project! (2023). Retrieved 27 April 2023, from https://qgis.org/en/site/

Welton-Mitchell, C., Awale, R., James, L., & Khanal, S. (2017). Investigating community resilience in Bhaktapur district and surrounding areas in Nepal following the 2015 earthquake. *16th World Conference on Earthquake Engineering*. https://www.eeri.org/images/archived/wp-content/uploads/2243-16WCEE-Nepal-Bhaktapur.pdf

Wong, M. S., Zhu, X., Abbas, S., Kwok, C. Y. T., & Wang, M. (2021). Optical Remote Sensing. In W. Shi, M. F. Goodchild, M. Batty, M.-P. Kwan, & A. Zhang (Eds.), *Urban Informatics* (pp. 315–344). Springer Singapore. https://doi.org/10.1007/978-981-15-8983-6_20

Zhang, R., Tang, X., You, S., Duan, K., Xiang, H., & Luo, H. (2020). A Novel Feature-Level Fusion Framework Using Optical and SAR Remote Sensing Images for Land Use/Land Cover (LULC) Classification in Cloudy Mountainous Area. *Applied Sciences*, *10*(8), 2928. https://doi.org/10.3390/app10082928